JOC The Journal of Organic Chemistry

Article

Cite This: J. Org. Chem. 2019, 84, 11649−11664

pubs.acs.org/joc

Azulichlorins and Benzocarbachlorins Derived Therefrom

Mario A. Noboa, Deyaa I. AbuSalim, and Timothy D. Lash*

Department of Chemistry, Illinois State University, Normal, Illinois 61790-4160, United States

Supporting Information

ABSTRACT: Acid-catalyzed condensation of azulidipyrrane aldehydes with a dihydrodipyrrin carbaldehyde afforded the first examples of azulichlorins. These macrocyclic products were isolated in a monoprotonated form, and the free bases proved to be somewhat unstable. The monocations were strongly diatropic, and proton NMR spectroscopy showed the internal C−H at ca. −2 ppm. Addition of TFA gave the related dications, but these exhibited significantly reduced aromatic ring currents. Reaction of an azulichlorin with *tert*-butyl hydroperoxide and KOH in dichloromethane/methanol gave a benzocarbachlorin and two related aldehydes. The UV−vis spectrum for the benzocarbachlorin showed a split Soret band at 414 and 430 nm, together with a strong chlorin-like absorption at 684 nm. The proton NMR spectrum indicated that the carbachlorin is strongly aromatic and the internal C−H was observed at −4.64 ppm. Addition of TFA afforded a C-protonated dication with a significantly increased diatropic ring current. The proton NMR spectrum, NICS calculations, and AICD plots indicated that the system favors a 22π electron delocalization pathway that runs through the fused benzo unit. Addition of TFA to the benzocarbachlorin aldehydes primarily led to the formation of monocations, and the generation of C-protonated dications was no longer favored due to the presence of electron-withdrawing formyl moieties.

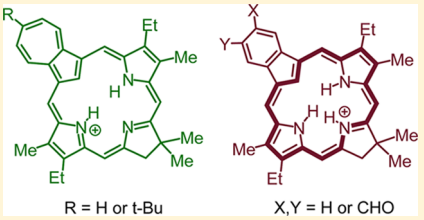

INTRODUCTION

Hydroporphyrins such as chlorins and bacteriochlorins (Figure 1) are widespread in nature and fulfill many important functions.[1−3] Most of the chlorophylls are magnesium chlorins,[3] while many bacteria utilize the iron(II) chlorin heme d (**1**, Figure 2) in the reduction of molecular oxygen to water.[4] Bacteriochlorophylls *a* and *b* are magnesium bacteriochlorins, and tolyporphin,[5] heme d_1,[6] and siroheme[7] are examples of isobacterichlorins. In addition, the marine worm *Bonellia viridis* generates the *gem*-dimethylchlorin bonellin (**2**) and this green pigment directs masculization of the larvae.[8] Bonellin also exhibits antitumor activity,[9] and chlorophyll-derived chlorins isolated from diatoms, sponges, tunicates, and mollusks have been shown to have antioxidant properties.[10] Chlorins have comparatively long wavelength absorptions near 650 nm, an attribute that is valued in the development of superior photosensitizers for applications in photodynamic therapy (PDT). For instance, verteporfin (Visudyne, **3**) is a photosensitizer that has been used to treat age-related macular degeneration[11] and has also been shown to have potential in atheroschlerotic plaque therapy.[12] *meso*-Tetrakis(3-hydroxyphenyl)chlorin (temoporfin) is similarly being used to treat squamous cell carcinomas,[13] and talaporfin (**4**) is being applied to the treatment of lung cancer.[14] Unsurprisingly, chlorins have been widely investigated and many synthetic routes to this system have been developed.[1,2,15] However,

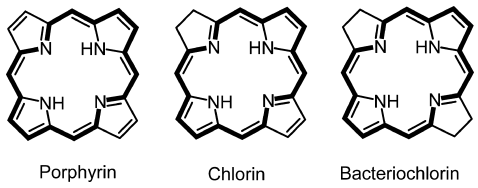

Figure 1. Structures of porphyrin, chlorin, and bacteriochlorin.

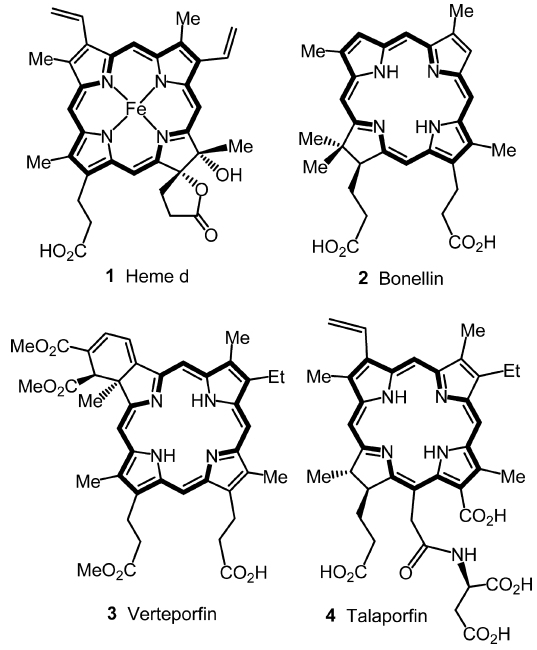

Figure 2. Examples of biologically active chlorins.

Received: June 13, 2019
Published: August 20, 2019

DOI: 10.1021/acs.joc.9b01578
J. Org. Chem. 2019, 84, 11649−11664

closely related chlorin-like systems have not been well studied even though these have the potential to possess equally valuable properties.[16]

Carbaporphyrinoid systems, where one or more of the core nitrogens within the porphyrin macrocycle have been replaced by carbon atoms, have diverse structural and spectroscopic properties[17] and display unusual reactivity such as the capacity to generate stable organometallic derivatives.[18] Examples of 2,3-dihydrocarbaporphyrins such as **5**−**8** (Figure 3) have been

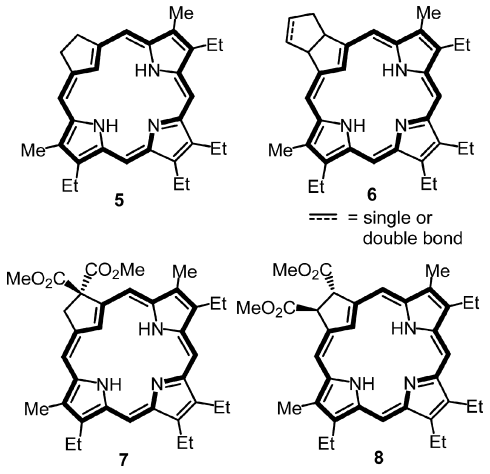

Figure 3. Previously reported carbachlorins.

reported[19−22] and these chlorin analogues all have strongly aromatic properties. In common with true chlorins, carbachlorins **5**−**8** show moderately strong absorptions near 650 nm but are relatively stable compounds compared to the tetrapyrrolic structures. Carbachlorins **5** and **8** only undergo oxidation to carbaporphyrins when heated with DDQ in toluene,[20,21] while the five-membered ring fused carbachlorins **6** resisted oxidation under any of the conditions examined.[19] This process is blocked altogether in the *gem*-diester **7**.[21] It is noteworthy that these structures only represent a single category of carbachlorin where the carbocyclic ring has been reduced. Carbachlorins **CC-c** and **CC-b** with reductions of pyrrole rings c and b, respectively, represent currently unknown examples of chlorin analogues, and the related benzocarbachlorins **BCC-c** and **BCC-b** have also hitherto not been explored (Figure 4). In addition, dihydroazuliporphyrins **AzC-c** and **AzC-b** are examples of previously unknown azulichlorin structures.

Azuliporphyrins **9** are porphyrin analogues that have an azulene unit instead of one of the pyrrole rings (Figure 5).[23] This system acts as a dianionic ligand and affords organometallic derivatives with Ni(II),[24] Pd(II),[24] Pt(II),[24] Ru(II),[25] Rh(III),[26] and Ir(III).[27] The first example of an azuliporphyrin was reported in 1997,[28] and this system was shown to have significantly reduced diatropic properties compared to porphyrins or carbaporphyrins.[29] The intriguing reactivity and spectroscopic properties of azuliporphyrins have led to the investigation of related porphyrinoid structures, including azulicorrole **10**,[30] azulisapphyrin **11**,[31] and the azulene-fused azacoronene analogue **12**.[32] Hence, the development of syntheses for azulichlorins and new classes of carbachlorins was considered to be desirable for the development of this field. In this paper, syntheses of azulichlorins belonging to the **AzC-c** class and related benzocarbachlorins belonging to

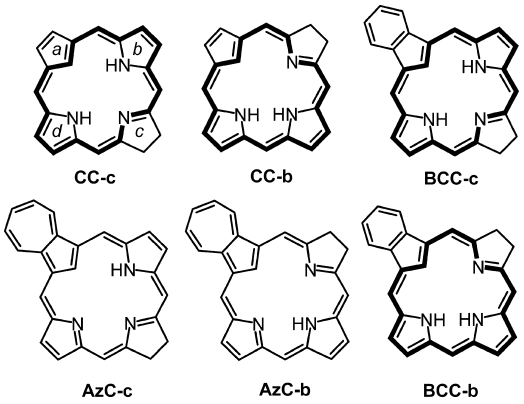

Figure 4. Proposed carbachlorin and azulichlorin systems.

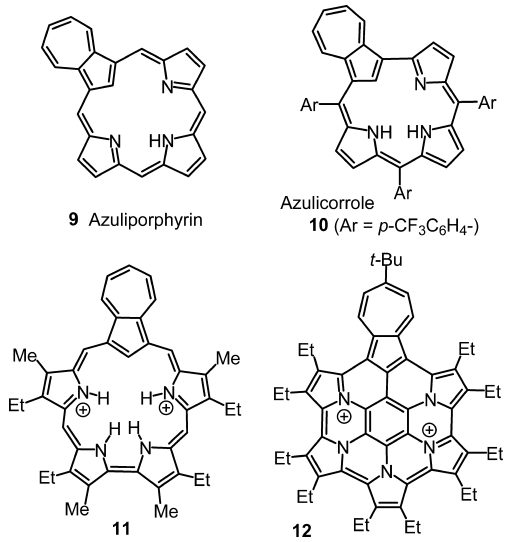

Figure 5. Examples of azulene-containing porphyrin analogues.

category **BCC-c** are reported and detailed spectroscopic and computational studies have been performed.[33]

RESULTS AND DISCUSSION

The "3 + 1" version of the MacDonald condensation is a versatile method for preparing diverse porphyrinoid structures.[34] Initially, dihydrotripyrrene **13** was targeted as a potential intermediate in the synthesis of carbachlorin analogues. In principle, cleavage of the *tert*-butyl ester protective groups, followed by condensation with monocyclic dialdehydes, would afford the desired macrocyclic products. Convenient syntheses of dihydrodipyrrins related to structure **14** have been reported by Jacobi and co-workers,[35−38] and these useful intermediates have been used to prepare a variety of chlorin[37,38] and bacteriochlorin products.[39] It was anticipated that functionalization of the terminal methyl unit

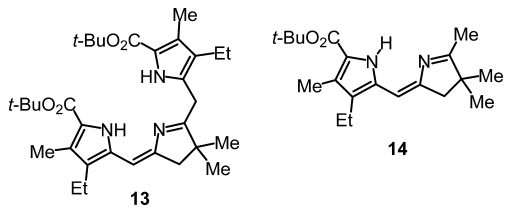

DOI: 10.1021/acs.joc.9b01578
J. Org. Chem. 2019, 84, 11649−11664

in **14**, followed by condensation with an α-unsubstituted pyrrole, would afford the required dihydrotripyrrene.

Heck coupling of iodopyrrole **15** with pentynoic acid **16** and catalytic $Pd(PPh_3)_4$ in refluxing triethylamine-acetonitrile gave lactone **17** in 87% yield (Scheme 1). The formation of *Z*-

Scheme 1. Synthesis of Dihydrodipyrrin Intermediates

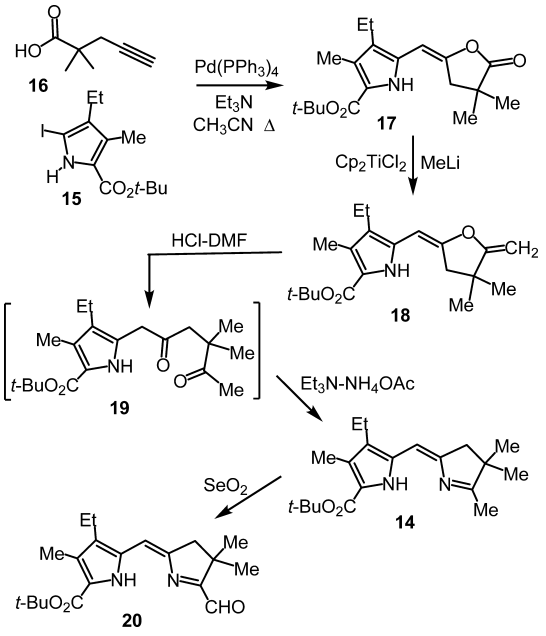

isomer **17** was confirmed by NOE difference proton NMR spectroscopy. These studies showed interactions between the N−H resonance and the lactone CH_2 unit that would only be observed in the *Z*-isomer. Furthermore, the bridge C−H weakly interacted with the CH_2 resonance for the ethyl substituent. Reaction of **17** with the Petasis reagent (dimethyl titanocene) in refluxing toluene afforded the related enol ether **18** in 76% yield. NOE difference proton NMR spectroscopy again confirmed that the *Z*-isomer had been obtained. The two protons attached to the exocyclic double bond gave 1H doublets at 4.02 and 4.40 ppm, and the upfield resonance was shown to correspond to the hydrogen atom that was orientated toward the *gem*-dimethyl unit. In a one-pot procedure, enol ether **18** was dissolved in DMF and hydrolyzed with 6 M hydrochloric acid to generate diketone **19**. This intermediate underwent a Paal−Knorr cyclization in situ with excess ammonium acetate and triethylamine at 55 °C, and following purification by flash chromatography on silica gel, dihydrodipyrrin **14** was isolated in 70% yield (Scheme 1). This product was shown to take on the desired *E*-geometry by NOE difference proton NMR spectroscopy as the resonance for the bridge C−H at 5.82 ppm correlated with the pyrrolene methylene unit at 2.58 ppm.

Attempts to functionalize the terminal methyl group of **14** with lead tetraacetate, *N*-bromosuccinimide, *N*-iodosuccinimide, or *N*-chlorosuccinimide led to decomposition. Jacobi had reported that related dihydrodipyrrins could be selectively oxidized with selenium dioxide to give aldehydes **20** and this transformation proved to be successful for **14** as well. Reaction of **14** with one equivalent of selenium dioxide in DMF-pyridine followed by purification using flash chromatography (silica gel, eluting with toluene) gave aldehyde **20** in 46% yield (Scheme 1). However, the formyl unit could not be reduced without destroying the dihydrodipyrrin, presumably due to the presence of a reactive imine unit.

Given the difficulties that had been encountered, it was necessary to develop an alternative strategy for the synthesis of carbachlorin-type structures such as azulichlorins **AzC-c**. As dihydropyrrin monoaldehyde was readily available, an alternative "2 + 2" strategy was designed, which made use of this intermediate. This necessitated the use of complementary azulidipyrrane aldehydes **21** (Scheme 2). Azulene was reacted

Scheme 2. Synthesis of Azulidipyrrane Carbaldehydes

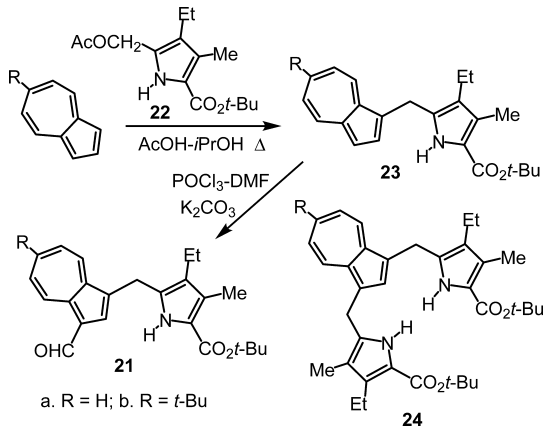

with one equivalent of acetoxymethylpyrrole **22** and acetic acid in refluxing isopropyl alcohol. Following column chromatography, azulidipyrrane **23a** was obtained as the major product, together with the related azulitripyrrane **24a**.[40,41] Condensation of 6-*tert*-butylazulene with **22** similarly gave azulidipyrrane **23b**, together with azulitripyrrane **24b** (Scheme 2). Initially, formylation of **23a** or **23b** using the Vilsmeier−Haack reaction ($POCl_3$/DMF) gave poor results because the acidic conditions cleaved the *tert*-butyl ester protective groups. However, when the reaction of **23a** was carried out in the presence of potassium carbonate, azulidipyrrane aldehyde **21a** was generated in 69% yield. Azulidipyrrane **23b** reacted similarly to afford the related aldehyde **21b** (Scheme 2).

Aldehydes **20** and **21a** were treated with TFA to cleave the *tert*-butyl ester protective groups, and the solutions were then diluted with acetic acid and further acidified with hydroiodic acid (Scheme 3). Although self-condensation of **20** or **21a** could potentially occur, only one macrocyclic product was identified resulting from the desired cross-condensation reaction. The reaction mixture was stirred at room temperature overnight, and the product was purified on a silica gel column. A green band was collected and further purified on a basic alumina column to give the monoprotonated azulichlorin

Scheme 3. Synthesis of Azulichlorins

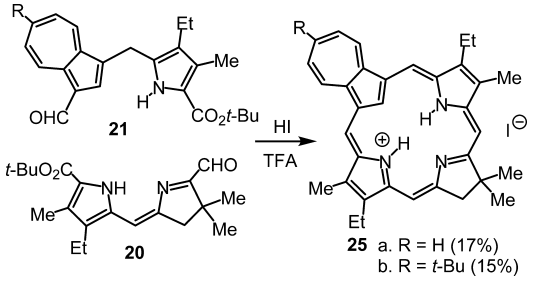

DOI: 10.1021/acs.joc.9b01578
J. Org. Chem. 2019, 84, 11649−11664

25a.HI in 17% yield. The proton NMR spectrum for **25a**H$^+$ in $CDCl_3$ (Figure 6) shows the internal C−H proton at −2.11

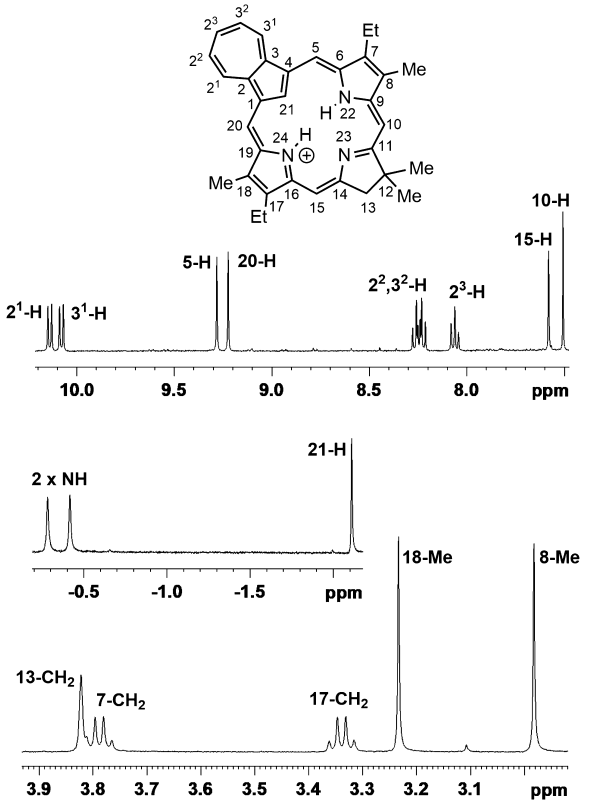

Figure 6. Proton NMR spectrum of azulichlorin **25a**.HI in $CDCl_3$.

ppm, and this result indicates that the monocation has a similar diamagnetic ring current to protonated azuliporphyrins. The *meso*-protons were shifted downfield to give four singlets at 7.51 (10-H), 7.58 (15-H), 9.22 (20-H), and 9.28 (5-H) ppm.

The UV−vis spectrum of azulichlorin **25a**H$^+$ gave a strong Soret band at 445 nm along with two weaker broad bands at 620 and 670 nm (Figure 7). When **25a**H$^+$ was exposed to triethylamine, a yellow solution corresponding to the free-base azulichlorin **25a** was generated (Scheme 4). The UV−vis spectrum of **25a** in 1% Et_3N/chloroform (Figure 7) showed substantial changes and the Soret band was lost, suggesting a

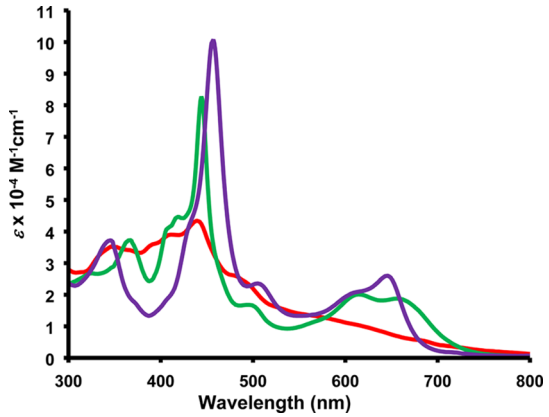

Figure 7. UV−vis spectra of azulichlorin **25a** in 1% $Et_3N/CHCl_3$ (free base, red line), $CHCl_3$ (monocation **25a**H$^+$, green line), and 5% TFA/$CHCl_3$ (dication **25a**H_2^{2+}, purple line).

decrease in aromaticity. The free-base form is somewhat unstable and slowly air-oxidized to give impure carbachlorins. The proton NMR spectra of **25a** in $Et_3N/CDCl_3$ or d_5-pyridine gave broad poorly resolved peaks. Addition of TFA afforded a diprotonated species **25a**H_2^{2+}, and the resulting UV−vis spectrum in 5% TFA/chloroform showed a strong Soret band at 457 nm and weaker absorptions at 345, 505, 605, and 645 nm (Figure 7). Interestingly, the proton NMR spectrum of **25a**H_2^{2+} showed a decrease in the diatropic ring current compared to the monoprotonated species as the internal C−H proton was only shifted upfield to 2.24 ppm, while the NH protons gave broad peaks at 1.26, 5.40, and 5.41 ppm. The *meso*-protons, however, were less affected, showing only minor shifts compared to **25a**H$^+$.

tert-Butylazulichlorin **25b** was synthesized under the same conditions from azulidipyrrane aldehyde **21b** and dihydrodipyrrin aldehyde **20**. As expected, azulichlorin **25b** was isolated as the monoprotonated species and gave a similar UV−vis spectrum to **25a**. The proton NMR spectrum for **25b**H$^+$ showed substantial diatropic character, although the internal C−H proton was slightly less shielded than the equivalent peak for **25a**H$^+$ and appeared at −1.46 ppm. However, the *meso*-protons were significantly deshielded compared to **25a**H, giving rise to four 1H singlets at 7.72, 7.83, 9.60, and 9.65 ppm. On balance, the presence of the *tert*-butyl substituent appears to enhance the diatropicity of the macrocycle. Similar observations were previously reported for *tert*-butyl substituted azuliporphyrins.[41]

Azuliporphyrins are susceptible to nucleophilic attack on the seven-membered ring and addition of pyrrolidine results in the reversible formation of aromatic carbaporphyrin adducts.[23,42] Addition of pyrrolidine to a solution of **25a**.HI gave a UV−vis spectrum that resembled an aromatic porphyrinoid structure. Specifically, a strong Soret band was observed at 408 nm, and a moderately strong chlorin-like absorption appeared at 677 nm (Figure 8). The proton NMR spectrum of **25a** with pyrrolidine in $CDCl_3$ showed the formation of a strongly aromatic species. The internal C−H was shifted upfield to −4.59 ppm and two broad NH resonances were observed at −2.16 and −2.12 ppm. The *meso*-protons were shifted downfield to give four 1H singlets at 8.34, 8.45, 9.49, and 9.52 ppm, and the resonances for the methyl substituents were also further deshielded giving rise to two 3H singlets at 3.27 and 3.36 ppm. The cycloheptatriene unit gave a 2H doublet at 7.70 and a 2H multiplet at 5.92−5.96 ppm. The results are consistent with the formation of the pyrrolidine adduct **26** where nucleophilic attack is favored at position 2^3 (Scheme 4). The reduced 13-CH_2 unit afforded an AB quartet ($^2J_{HH}$ = 16.3 Hz) for 2H at 4.39−4.47 ppm. This arises because the presence of the pyrrolidine unit differentiates the two faces of the macrocycle, and this leads to geminal coupling between the two protons.

In earlier work, azuliporphyrins had been reported to undergo oxidative ring contractions to generate benzocarbaporphyrins[42,43] and it was proposed that this transformation was triggered by initial nucleophilic attack onto the seven-membered ring. In a typical procedure, azuliporphyrins were reacted with *tert*-butyl hydroperoxide and KOH at room temperature. The same synthetic methodology was used to convert azulichlorin **25a** into the first examples of benzocarbachlorins (Scheme 4). Azulichlorin **25a** was reacted with potassium hydroxide and *tert*-butyl hydroperoxide in dichloromethane/methanol at room temperature. Following workup, the residue was chromatographed on a grade 3 alumina

DOI: 10.1021/acs.joc.9b01578
J. Org. Chem. 2019, 84, 11649−11664

Scheme 4. Protonation of Azulichlorins and Ring Contraction To Give Benzocarbachlorins

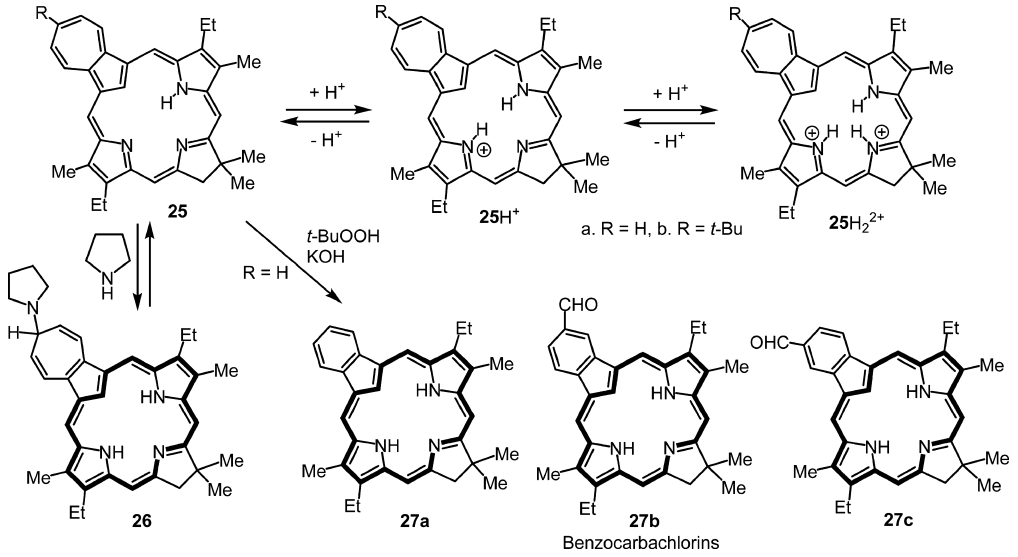

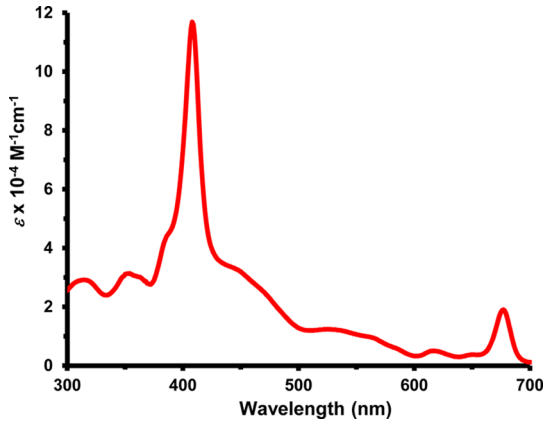

Figure 8. UV−vis spectrum of azulichlorin **25a** in 1% pyrrolidine/$CHCl_3$ showing the formation of carbachlorin adduct **26**.

column, eluting initially with 30% dichloromethane/hexanes, and an orange band was collected. Following recrystallization from chloroform/hexanes, benzocarbachlorin **27a** was obtained in 24% yield as a yellow-brown powder. A second major orange band was collected corresponding to a mixture of two isomeric benzocarbachlorin aldehydes **27b** and **27c** in 37−46% yield (Scheme 4).

The proton NMR spectrum for benzocarbachlorin **27a** in $CDCl_3$ showed the presence of a strong diamagnetic ring current (Figure 9). The internal C−H proton was observed at −4.64 ppm, and the N−H protons gave broad peaks at −2.63 and −2.58 ppm. The external *meso*-protons were shifted downfield to give four 1H singlets at 8.47 (10-H), 8.59 (15-H), 9.72 (20-H), and 9.76 (5-H) ppm. The carbon-13 NMR spectrum showed the internal CH at 111.4 ppm, while the *meso*-carbons appeared at 90.2 (C-10), 92.1 (C-15), 101.3 (C-20), and 101.6 (C-5) ppm. The UV−vis spectrum of benzocarbachlorin **27a** in 1% Et_3N/chloroform produced a split Soret band at 414 and 430 nm, together with a strong absorption at 684 nm that is characteristic of chlorin-type structures (Figure 10).

Addition of small amounts of TFA generated a monocationic species **27a**H^+ (Scheme 5). The UV spectrum for a solution of **27a** with 0.1% TFA/$CHCl_3$ showed that a new

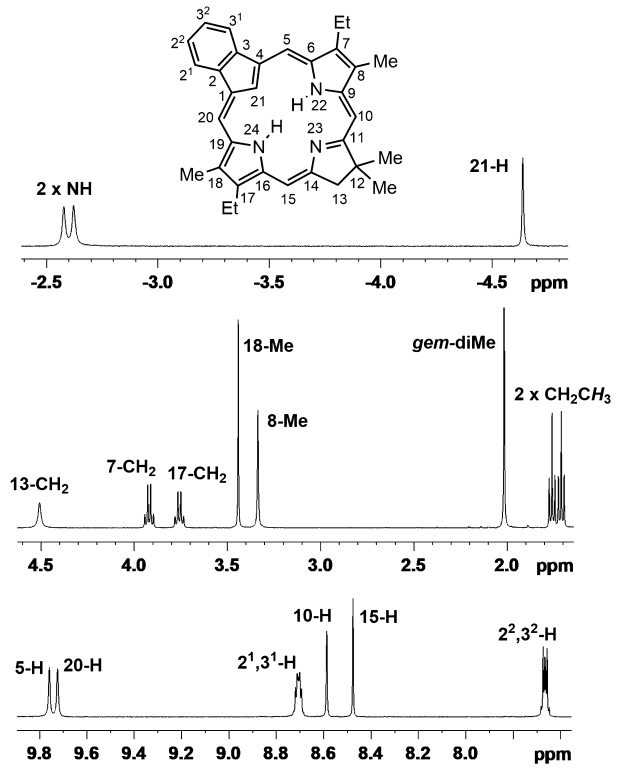

Figure 9. Proton NMR spectrum of benzocarbachlorin **27a** in $CDCl_3$.

species had been partially formed as a new absorption band had emerged at 717 nm. In 0.2% TFA/chloroform, this species predominated but a new band started to emerge at 800 nm. In 5% TFA/chloroform, the carbachlorin was completely converted into the latter form, and this was assigned to the dicationic structure **27a**H_2^{2+}. The dication gave a strong Soret band at 404 nm, in addition to the long wavelength absorption at 800 nm (Figure 10). The proton NMR spectrum for dication **27a**H_2^{2+} in TFA/$CDCl_3$ confirmed that C-protonation had occurred and indicated that the diatropicity of the carbachlorin system had been increased. The internal CH_2 resonance was observed upfield at −6.77 ppm, while the *meso*-protons were shifted downfield to give singlets at 9.47, 9.64,

DOI: 10.1021/acs.joc.9b01578
J. Org. Chem. 2019, 84, 11649−11664

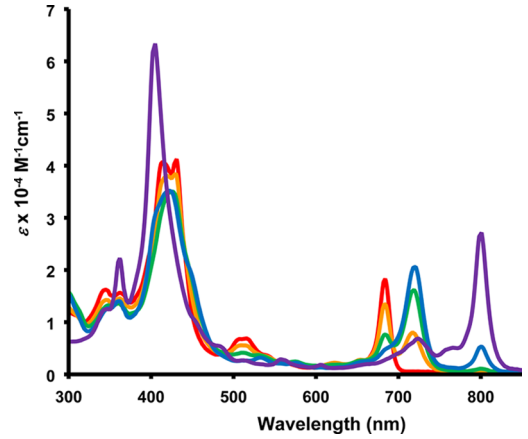

Figure 10. UV−vis spectra of benzocarbachlorin in $CHCl_3$ (free base, red line), 0.1% TFA/$CHCl_3$ (orange line), 0.2% TFA/$CHCl_3$ (green line), 0.5% TFA/$CHCl_3$ (blue line), and 5% TFA/$CHCl_3$ (dication **27a**H_2^{2+}, purple line).

Scheme 5. Protonation of Benzocarbachlorins

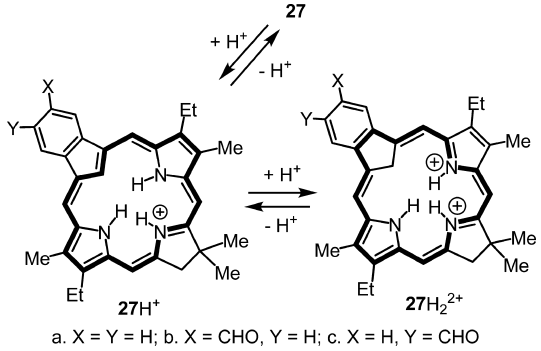

11.120, and 11.126 ppm. The chemical shifts for the methyl substituents were also shifted downfield by ca. 0.26 ppm, which also implies that a larger macrocyclic ring current is present. Major changes were observed for the chemical shifts of the benzo protons. In the free-base form, the 2,^{1}3^1-protons gave a multiplet at 8.68−8.73 ppm and the 2,^{2}3^2-protons appeared at 7.65−7.68 ppm, but these resonances were shifted downfield for **27a**H_2^{2+} to give multiplets at 10.09−10.12 ppm and 8.74−8.78 ppm, respectively. These shifts indicate that the global ring current passes through the benzene ring and that a 22π electron pathway plays a significant role (see computational results below). Similar conjugation pathways have been postulated for protonated benzocarbaporphyrins and naphthocarbaporphyrins.[44,45] The carbon-13 NMR spectrum for **27a**H_2^{2+} showed the internal CH_2 at 32.0 ppm, while the *meso*-carbons appeared at 101.2, 103.2, and 105.8 ppm (the latter resonance corresponds to both the 5- and 20-CHs).

Attempts to separate benzocarbachlorin aldehydes **27b** and **27c** were unsuccessful, and spectroscopic characterization was performed on the isomeric mixture. The proton NMR spectrum of **27b,c** in $CDCl_3$ showed that the two isomers were present in a 50/50 mixture, and both forms showed the presence of strong diamagnetic ring currents. The internal C−H protons were observed at −4.70 and −4.69 ppm, while the *meso*-protons gave rise to a series of singlets between 8.43 and 9.55 ppm. The aldehyde protons gave a singlet at 10.28 ppm. The UV−vis spectrum of **27b,c** gave a strong Soret band at 442 nm, together with small Q bands at 530, 557, and 616 nm and a stronger chlorin-type absorption at 676 nm (Figure 11). In 0.1% TFA/$CHCl_3$, a new species was formed, which

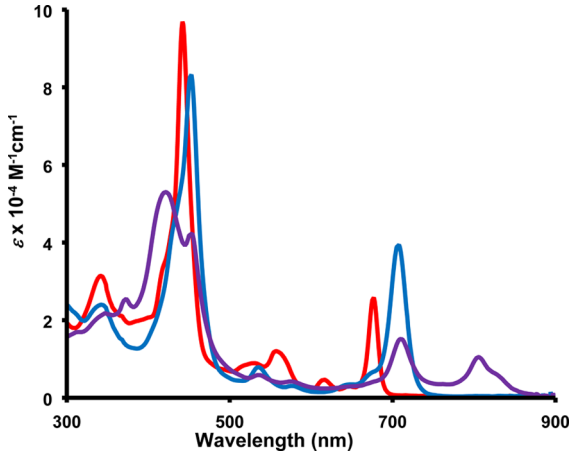

Figure 11. UV−vis spectra of benzocarbachlorincarbaldehydes **27b,c** in $CHCl_3$ (free bases, red line), 1% TFA/$CHCl_3$ (monocations **27b,c**H^+, blue line), and 50% TFA/$CHCl_3$ (mixture of monocations **27b,c**H^+ and dications **27b,c**H_2^{2+}, purple line).

afforded a Soret band at 450 nm and a strong absorption at 707 nm, and this was assigned to monocation **27b,c**H^+ (Scheme 5). However, further addition of TFA did not initially show any significant changes. Benzocarbachlorin **27a** was completely converted into the dicationic species **27a**H_2^{2+} in 5% TFA/$CHCl_3$, but benzocarbachlorins **27a,b** only showed trace amounts of the related dications in 10% TFA/chloroform (Figure 11). Even in 50% TFA/chloroform solutions, conversion to **27b,c**H_2^{2+} was incomplete. The presence of electron-withdrawing groups on the benzene ring apparently inhibits the second protonation step, indicating that there must be a significant electronic interaction between the benzo unit and the porphyrinoid macrocycle in these dicationic structures. This differs from the free-base and monocationic forms, where the benzo units appear to be effectively disconnected from the macrocyclic π-system. The proton NMR spectrum of **27b,c**H^+ in $CDCl_3$ containing a trace amount of TFA showed a downfield shift to the internal C−H protons from −4.7 to −2.0 ppm, and the *meso*-protons gave rise to singlets between 7.96 and 9.67 ppm. These results indicate that the macrocyclic ring currents for the free base and monoprotonated porphyrinoids are very similar. The aldehyde moiety afforded a singlet at 10.20 ppm.

Computational studies were also conducted on unsubstituted azulichlorins **AzC-c** and benzocarbachlorins **BCC-c** and these provide further insights into these novel chlorin analogues. A series of tautomers were examined for the free-base and protonated forms for each system. The structures were optimized using B3LYP with the triple-ζ basis set 6-311++G(d,p).[46] Four tautomers for the free-base forms of **AzC-c** were considered and these are designated according to the position of the proton as **AzC-c-22H**, **AzC-c-23H**, **AzC-c-5H**, and **AzC-c-10H** (Table 1). All four structures are essentially planar. The relative energies were assessed using three different functionals, B3LYP, M06-2X, and B3LYP-D3,[47,48] and the relative Gibbs free energy was determined using B3LYP. The relative ΔG values were consistently very similar to the relative ΔE values, demonstrating that entropic factors are not significant. The calculations showed that **AzC-c-22H** is the

DOI: 10.1021/acs.joc.9b01578
J. Org. Chem. 2019, 84, 11649−11664

Table 1. Calculated Relative Energies (kcal/mol) and NICS Values (ppm) for Free-Base Unsubstituted Azulichlorin Tautomers

	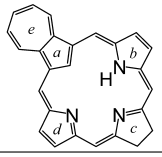	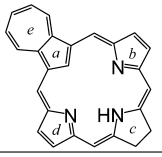	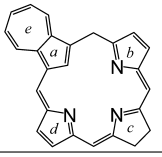	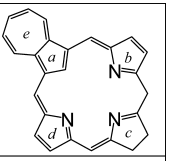
Molecule	**AzC-c-22H**	**AzC-23H**	**AzC-c-5H**	**AzC-10H**
ΔG (298 K)	0.00	+0.12	+28.36	+25.50
ΔE (B3LYP/ **M06-2X**/ B3LYP-D3)	(0.00/ **0.00**/ 0.00)	(-1.27/ **-3.53**/ -1.38)	(+30.23/ **+27.89**/ +30.83)	(+27.00/ **+23.01**/ +27.74)
NICS(0)/NICS(1)$_{zz}$	-4.07/-9.38	-1.69/-2.95	+0.35/+3.27	+1.72/+6.53
NICS(*a*)/NICS(1*a*)$_{zz}$	-14.07/-39.27	-13.46/-38.37	-14.10/-40.59	-13.15/-38.11
NICS(*b*)/NICS(1*b*)$_{zz}$	-6.59/-16.49	-1.36/-9.27	+1.78/-3.74	-1.36/-9.45
NICS(*c*)/NICS(1*c*)$_{zz}$	+3.57/+4.22	+0.54/+4.22	+1.62/+0.02	+1.23/-1.54
NICS(*d*)/NICS(1*d*)$_{zz}$	-0.08/-6.88	-1.36/-9.27	-1.50/-9.66	-0.61/-47.51
NICS(*e*)/NICS(1*e*)$_{zz}$	-0.92/-9.27	-1.90/-11.89	-3.71/-16.09	-3.44/-15.57

most stable, yet **AzC-c-23H** is only slightly higher in energy. Although the conjugation pathway in **AzC-c-22H**, which passes through an imine unit within the reduced ring, would be expected to be favored over the alternative pathway in **AzC-c-23H**, which passes through an amine-type nitrogen, the former species has more steric congestion because the two internal hydrogens are adjacent to one another. The other two tautomers, which have interrupted conjugation pathways due to the presence of methylene bridges, are much higher in energy (Table 1). Nucleus-independent chemical shift (NICS) calculations were carried out[49] using CAM-B3LYP to assess the aromatic properties of these structures. Large negative values correspond to highly shielded regions that result from aromatic ring currents, while positive values correspond to deshielded regions. In this study, NICS(0) and NICS$_{zz}$(1) calculations were conducted. Standard NICS calculations consider the effects due to σ and π electrons and may not always reliably assess aromatic properties, but NICS$_{zz}$ primarily measures the effects due to the π system. NICS$_{zz}$ calculations were performed 1 Å above the ring. It should be noted that the numerical values obtained using NICS$_{zz}$(1) are much larger than those obtained using NICS(0), but the porphyrinoids examined in these studies showed similar trends using both techniques. To avoid confusion, only the NICS(0) values will be discussed. **AzC-c-22H** exhibits moderate global diatropicity, giving an NICS(0) value of −4.07 ppm. The NICS values for rings *a* and *b* are strongly negative, demonstrating that the ring current primarily runs through the outside of these rings, but rings *c* and *d* give low negative or positive results showing that the pathway runs through the inside of these subunits. In addition to the NICS calculations, anisotropy of induced current density (AICD)[50] was used to assess all of the calculated structures, and the plot for **AzC-c-22H** showed that bifurcated pathways were present, which exclude the cycloheptatriene moiety (Figure 12). The global ring current in **AzC-c-23H** is virtually absent, presumably due to the necessity for this conjugation pathway to pass through the amine-type nitrogen.

Protonation gives rise to monocationic and dicationic species. Eight possible monocationic tautomers were considered (Table 2), and **AzC-c-22,24H$^+$** was calculated to be by far the most favored form. **AzC-c-22,23H$^+$** was ca. 10 kcal/mol higher in energy, while the remaining *meso*-protonated structures were 22−38 kcal/mol higher in energy. **AzP-c-22,23H$^+$** is less favored due to steric crowding and the

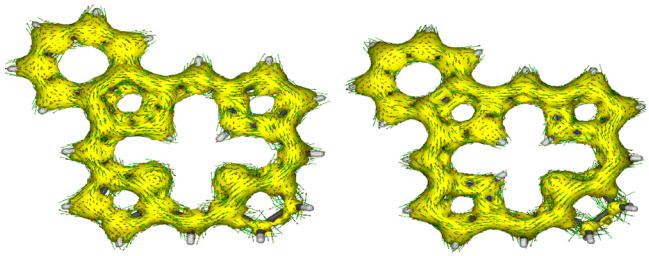

Figure 12. AICD plots (isovalues = 0.05) of azulichlorin **AzC-c-22H** and monocation **AzC-c-22,24H$^+$**.

necessity for the π-conjugation pathways to pass through the amine-type nitrogen. Nevertheless, this tautomer has a significant NICS(0) value of −4.17 ppm and therefore would have diatropic character. The favored tautomer, **AzC-c-22,24H$^+$**, gave a larger NICS(0) value of −6.85 ppm and rings *a*, *b*, and *d* all gave large negative values, demonstrating that the favored aromatic delocalization pathways run through the outside of these rings. This suggests that the pathway shown in structure **28a** (Figure 13) is favored, although the small negative values calculated for the seven-membered ring (ring *e*) are rather small and therefore not consistent with tropylium character. However, the AICD plot for this tautomer (Figure 12) indicates that π-conjugation extended through the seven-membered ring and instead is suggestive of contributions from 23-atom delocalized structure **28b**. In fact, computational studies on azuliporphyrins also suggest that tropylium character is not favored in the free-base and monoprotonated forms,[51] even though this interpretation is generally used to explain the properties of azuliporphyrins.[42] Attempts to rationalize the conjugation pathways in terms of resonance led to the proposal of similar somewhat unlikely canonical forms, and it was concluded that azuliporphyrins cannot be satisfactorily assessed in this fashion.[51] The calculated bond lengths for the favored free-base and monocations **AzC-c-22H** and **AzC-c-22,24H$^+$** showed very little variation for the individual bonds in the seven-membered ring apart from the position for ring fusion. In fact, this bond (C2−C3) was 0.078 Å or 0.067 Å longer, respectively, for these two species. A series of diprotonated dications were also considered (Table 3) and **AzC-c-22,23,24H^{2+}** was unambiguously favored over the C-protonated tautomers. The system retained substantial global diatropicity (NICS(0) = −5.47 ppm), but this is

DOI: 10.1021/acs.joc.9b01578
J. Org. Chem. 2019, 84, 11649−11664

Table 2. Calculated Relative Energies (kcal/mol) and NICS Values (ppm) for Tautomers of Monoprotonated Azulichlorins

	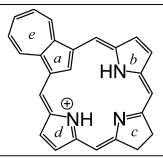	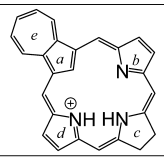	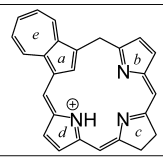	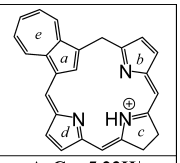
Molecule	**AzC-c-22,24H$^+$**	**AzC-c-22,23H$^+$**	**AzC-c-5,24H$^+$**	**AzC-c-5,23H$^+$**
ΔG (298 K)	0.00	+10.92	+22.55	+31.60
ΔE (B3LYP/ **M06-2X**/ B3LYP-D3)	(0.00/ **0.00**/ 0.00)	(+10.56/ **+9.54**/ +10.73)	(+24.00/ **+22.20**/ +24.92)	(+33.96/ **+34.68**/ +34.76)
NICS(0)/NICS(1)$_{zz}$	-6.85/-17.25	-4.17/-9.82	+0.10/+2.09	-1.92/-3.31
NICS(*a*)/NICS(1*a*)$_{zz}$	-10.76/-28.83	-9.24/-25.74	-9.60/-28.13	-9.48/-28.48
NICS(*b*)/NICS(1*b*)$_{zz}$	-8.30/-20.72	-1.56/-10.51	+2.88/-1.23	+4.00/+0.92
NICS(*c*)/NICS(1*c*)$_{zz}$	+5.00/+5.81	+1.82/+5.52	+1.92/+0.21	+1.93/+5.92
NICS(*d*)/NICS(1*d*)$_{zz}$	-8.31/-20.73	-8.97/-19.50	-7.44/-17.93	-3.16/-13.11
NICS(*e*)/NICS(1*e*)$_{zz}$	-2.91/-16.14	-3.10/-16.43	-4.83/-19.38	-4.00/-17.44
	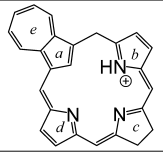	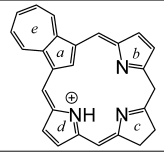	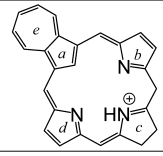	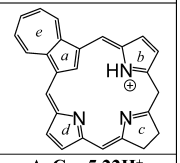
Molecule	**AzC-c-5,22H$^+$**	**AzC-c-10,24H$^+$**	**AzC-c-10,23H$^+$**	**AzC-c-5,22H$^+$**
ΔG (298 K)	+32.35	+20.34	+31.99	+24.75
ΔE (B3LYP/ **M06-2X**/ B3LYP-D3)	(+34.34/ **+37.70**/ +35.27)	(+22.65/ **+20.05**/ +23.68)	(+33.27/ **+30.38**/ +34.26)	(+26.91/ **+24.38**/ +28.02)
NICS(0)/NICS(1)$_{zz}$	-3.29/-6.87	+1.03/+4.47	+0.94/+4.26	+1.20/+4.86
NICS(*a*)/NICS(1*a*)$_{zz}$	-8.49/-26.04	-9.23/-26.98	-9.49/-28.15	-7.83/-23.79
NICS(*b*)/NICS(1*b*)$_{zz}$	-8.89/-21.34	-0.67/-7.73	-3.22/-12.88	-8.32/-19.82
NICS(*c*)/NICS(1*c*)$_{zz}$	+3.74/+4.74	+1.65/-0.92	+0.37/+2.02	+1.59/-0.48
NICS(*d*)/NICS(1*d*)$_{zz}$	-1.19/-9.73	-6.47/-15.59	-2.71/-11.63	+0.83/-4.26
NICS(*e*)/NICS(1*e*)$_{zz}$	-3.78/-17.53	-4.44/-18.53	-4.28/-18.26	-4.45/-18.61

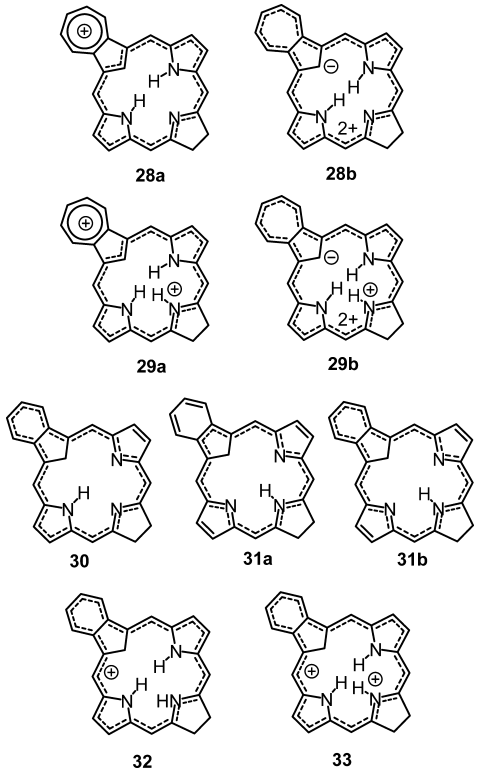

Figure 13. Potential conjugation pathways in selected azulichlorin and benzocarbachlorin structures.

reduced compared to monocation **AzC-22,24H$^+$** in agreement with the proton NMR spectra obtained for azulichlorins **25a** and **25b**. Rings *a*, *b*, and *d* all gave significant negative NICS values, suggesting that the ring current passes through the periphery of these rings. The seven-membered ring also gives a substantial negative NICS value, potentially indicating that this species possesses tropylium character, and the results are consistent with the conjugation pathway shown in structure **29a** (Figure 13). However, the AICD plot for **AzC-c-22,23,24H^{2+}** (Figure 14) indicates that the global conjugation pathway extends around the periphery of the seven-membered ring. The calculated bond length for C2−C3 is 1.449 Å, which also indicates that this bond has substantial single bond character, although it is slightly shorter than the equivalent bond in **AzC-c-22H**. Again, it is only possible to postulate a rather unconventional resonance contributor **29b** for this species.

Eight tautomers of free-base benzocarbachlorin **BCC-c** were considered and unsurprisingly, **BCC-c-22,24H** was the most favored (Table 4). This tautomer is highly diatropic (NICS(0) = −11.70 ppm) and the rings *b* and *c* give large negative NICS values, which demonstrate that the macrocyclic ring current runs around the outside of these rings taking the inside track for rings *a* and *c*. This interpretation is confirmed by the AICD plot for this tautomer (Figure 15). Nonaromatic tautomers with CH_2 bridges were 21.46−32.32 kcal/mol higher in energy. **BCC-c-22,23H** is approximately 10−12 kcal/mol less stable due to the presence of a less favorable conjugation pathway that runs through an amine-type nitrogen and because the two NHs are adjacent to one another. Tautomers **BCC-c-21,22H** and **BCC-c-21,23H** have internal methylene units and π-conjugation can occur through the exterior of ring *a* (18π electron pathway) or through the fused benzo unit (22π electron pathway). Both forms are much higher in energy but

DOI: 10.1021/acs.joc.9b01578
J. Org. Chem. 2019, 84, 11649−11664

Table 3. Calculated Relative Energies (kcal/mol) and NICS Values (ppm) for Azulichlorin Dications

	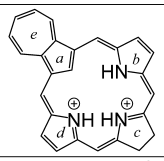	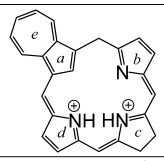	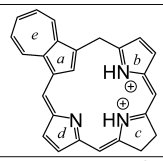	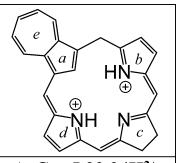
Molecule	**AzC-c-22,23,24H^{2+}**	**AzC-c-5,23,24H^{2+}**	**AzC-c-5,22,23H^{2+}**	**AzC-c-5,22,24H^{2+}**
ΔG (298 K)	0.00	+18.21	+24.61	+10.32
ΔE (B3LYP/ **M06-2X**/ B3LYP-D3)	(0.00/ **0.00**/ 0.00)	(+19.54/ **+18.91**/ +20.50)	(+25.99/ **+30.04**/ +27.01)	(+11.70/ **+14.08**/ +12.59)
NICS(0)/NICS(1)$_{zz}$	-5.47/-8.26	-0.78/-0.07	-3.19/-5.87	-2.71/-4.88
NICS(*a*)/NICS(1*a*)$_{zz}$	-5.58/-16.18	-5.40/-15.85	-0.91/-8.85	-7.05/-19.78
NICS(*b*)/NICS(1*b*)$_{zz}$	-9.48/-18.99	+5.17/+3.94	-10.54/-19.40	-6.15/-15.04
NICS(*c*)/NICS(1*c*)$_{zz}$	+2.85/+4.91	+0.71/+2.90	+2.39/+6.03	+3.22/+3.16
NICS(*d*)/NICS(1*d*)$_{zz}$	-9.48/-18.98	-9.39/-20.02	+1.32/+23.57	-8.54/-20.85
NICS(*e*)/NICS(1*e*)$_{zz}$	-4.12/-19.29	-4.92/-20.83	-4.27/-19.09	-4.80/-20.15
	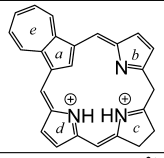	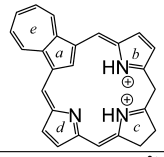	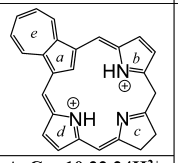	
Molecule	**AzC-c-10,23,24H^{2+}**	**AzC-c-10,22,23H^{2+}**	**AzC-c-10,22,24H^{2+}**	
ΔG (298 K)	+17.72	+21.29	+2.66	
ΔE (B3LYP/ **M06-2X**/ B3LYP-D3)	(+19.09/ **+17.19**/ +20.30)	(+22.57/ **+20.04**/ +23.76)	(+4.04/ **+2.75**/ +5.00)	
NICS(0)/NICS(1)$_{zz}$	+0.76/+3.87	+2.51/+9.20	+0.60/+3.37	
NICS(*a*)/NICS(1*a*)$_{zz}$	-5.19/-14.52	-5.06/-14.59	-7.05/-17.80	
NICS(*b*)/NICS(1*b*)$_{zz}$	-2.21/-11.00	-8.92/-17.83	-5.13/-12.88	
NICS(*c*)/NICS(1*c*)$_{zz}$	+0.10/+1.28	-1.12/-1.27	+1.88/0.00	
NICS(*d*)/NICS(1*d*)$_{zz}$	-8.60/-18.83	-0.77/-7.34	-7.81/-18.45	
NICS(*e*)/NICS(1*e*)$_{zz}$	-5.00/-20.95	-5.40/-21.97	-5.13/-21.35	

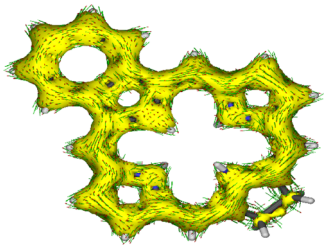

Figure 14. AICD plot (isovalue = 0.05) of azulichlorin dication **AzC-c-22,23,24H^{2+}**.

nevertheless are strongly aromatic species. **BCC-c-21,22H** has an NICS(0) value of −8.92 ppm and shows an increased NICS value for the benzo unit, indicating that the 22π conjugation circuit (structure **30**) is an important contributor. This pathway is also evident in the AICD plot (Figure 15). The structure of **BCC-c-21,23H** disrupts the 6π electron arene structure and while an 18π electron circuit is still possible in this tautomer, this route (**31a**) appears to be overwhelmed by the 22π electron pathway **31b**. Both of these pathways must pass through an amine-type nitrogen for **BCC-c-21,23H**, so it is remarkable that the global aromatic character (NICS(0) = −11.90 ppm) is substantially larger than is seen for **BCC-c-21,22H**. Nevertheless, the proposed π-circuit is evident in the AICD plot for this species (Figure 15).

Nine tautomers of monoprotonated **BCC** were analyzed and the most stable form proved to be C-protonated **BCC-c-21,22,24H$^+$** rather than the expect N-protonated structure **BCC-c-22,23,24H$^+$** (Table 5). The more stable tautomer is highly diatropic with an NICS(0) value of −13.08 ppm and rings *a*, *b*, *d*, and *e* all gave large negative NICS values. These results were consistent with the 23-atom 22π electron delocalization pathway shown in structure **32**, an outcome that is also supported by AICD calculations (Figure 15). The C1−C2 and C3−C4 bonds, which connect the benzo unit to the rest of the macrocycle, are ca. 0.04 Å shorter than in the free base demonstrating increased conjugative connectivity, although more pronounced bond length alternations emerge in the arene unit. The NICS(0) value for **BCC-c-22,23,24H$^+$**, while substantial, is less than −8 ppm indicating reduced aromaticity, and the results suggest that a porphyrin-like 18π electron pathway is favored for this species. It was not possible to obtain the proton NMR spectrum for monoprotonated benzocarbachlorin **27a**, but the related aldehydes **27b,c** gave conventional N-protonated monocations **27b,c**H$^+$ (Scheme 5) in contradiction to the computational results. In tautomer **BCC-c-22,23,24H$^+$**, the benzo unit is effectively disconnected from the global conjugation pathways and the presence of an electron-withdrawing formyl moiety would not significantly affect the stability of the monocation. However, the presence of an aldehyde substituent on the benzo fragment of **BCC-c-21,22,24H$^+$** would directly interact with the 22π electron delocalization pathway and would thereby destabilize the structure. Hence, the N-protonated tautomer is more favored under these circumstances. The alternative C-protonated monocation **BCC-c-21,22,23H$^+$** was calculated to be >12 kcal/mol higher in energy, presumably due to unfavorable steric interactions between the adjacent NHs. In addition, the core arrangement in **BCC-c-21,22,24H$^+$** is set up for much more favorable hydrogen bonding interactions. The remaining tautomers are protonated onto one of the *meso*-carbon bridges and four of the six structures show increases in the relative energies that were close to 30 kcal/mol. However, **BCC-c-**

DOI: 10.1021/acs.joc.9b01578
J. Org. Chem. 2019, 84, 11649−11664

Table 4. Calculated Relative Energies (kcal/mol) and NICS Values (ppm) for Benzocarbachlorin Tautomers

	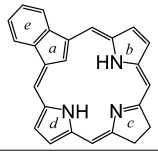	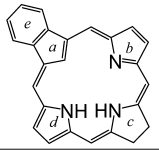	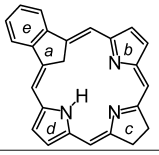	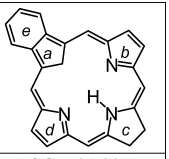
Molecule	**BCC-c-22,24H**	**BCC-c-22,23H**	**BCC-c-21,22H**	**BCC-c-21,23H**
ΔG (298 K)	0.00	+12.15	+15.83	+21.70
ΔE (B3LYP/ **M06-2X**/ B3LYP-D3)	(0.00/ **0.00**/ 0.00)	(+11.62/ **+9.71**/ +11.80)	(+16.73/ **+16.49**/ +16.90)	(+21.79/ **+23.49**/ +21.70)
NICS(0)/NICS(1)$_{zz}$	-11.70/-30.07	-6.48/-15.84	-8.92/-20.93	-11.90/-29.35
NICS(*a*)/NICS(1*a*)$_{zz}$	+2.46/+1.18	+2.79/+3.19	-9.89/-30.30	-13.62/-40.75
NICS(*b*)/NICS(1*b*)$_{zz}$	-13.28/-31.95	-3.57/-15.03	+0.20/-7.88	-2.45/-13.68
NICS(*c*)/NICS(1*c*)$_{zz}$	+6.98/+10.71	+2.64/+7.90	+5.85/+9.54	+6.91/+16.99
NICS(*d*)/NICS(1*d*)$_{zz}$	-13.30/-31.61	-13.70/-28.54	-14.39/-35.05	-2.45/-13.68
NICS(*e*)/NICS(1*e*)$_{zz}$	-6.27/-22.41	-6.51/-22.92	-9.49/-30.60	-8.86/-29.52
	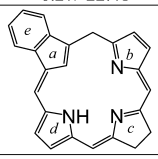	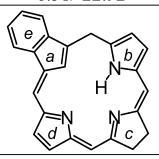	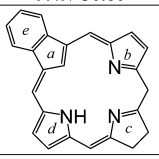	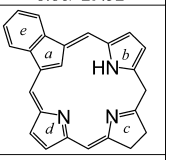
Molecule	**BCC-c-5,24H**	**BCC-c-5,22H**	**BCC-c-10,24H**	**BCC-c-10,22H**
ΔG (298 K)	+25.27	+29.23	+22.87	+25.48
ΔE (B3LYP/ **M06-2X**/ B3LYP-D3)	(+26.97/ **+24.59**/ +27.98)	(+31.36/ **+29.81**/ +32.32)	(+24.98/ **+21.46**/ +26.02)	(+27.65/ **+23.89**/ +28.74)
NICS(0)/NICS(1)$_{zz}$	-0.97/-0.47	-1.25/-1.28	+0.17/+2.40	+0.58/+3.47
NICS(*a*)/NICS(1*a*)$_{zz}$	+2.49/+2.64	+5.65/+9.31	+1.06/-0.50	+1.14/-0.36
NICS(*b*)/NICS(1*b*)$_{zz}$	+0.13/-7.45	-12.11/-26.27	-2.62/-12.18	-11.38/-25.07
NICS(*c*)/NICS(1*c*)$_{zz}$	+2.03/+1.76	+2.12/+2.27	+1.73/+0.64	+1.62/-0.08
NICS(*d*)/NICS(1*d*)$_{zz}$	-10.75/-24.58	-0.15/-7.46	-10.09/-22.69	-1.36/-9.04
NICS(*e*)/NICS(1*e*)$_{zz}$	-6.94/-23.43	-6.22/-21.74	-7.42/-24.43	-7.46/-24.65

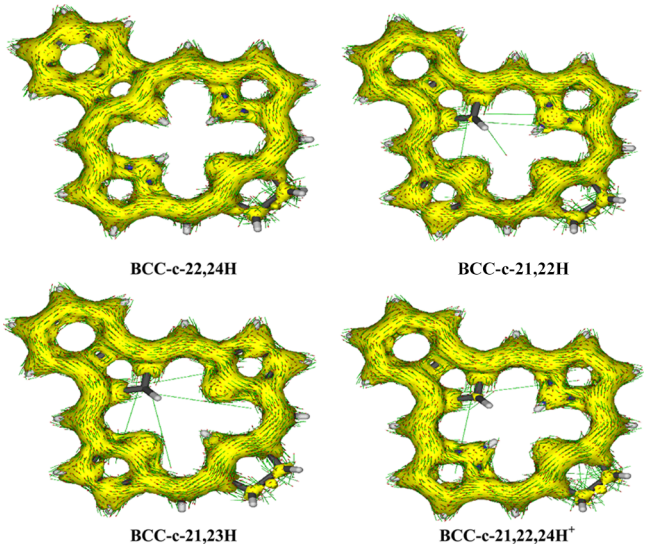

Figure 15. AICD plots (isovalues = 0.05) for benzocarbachlorin tautomers **BCC-c-22,24H**, **BCC-c-21,22H**, and **BCC-c-21,23H** and for monocation **BCC-c-21,22,24H**$^+$. **BCC-c-22,24H** shows a porphyrin-like 18π electron delocalization pathway that bypasses the benzo unit. However, the remaining structures favor 22π electron pathways that run around the benzo moiety.

22,23,24H$^+$ and **BCC-c-22,23,24H**$^+$ were far more accessible species (relative energies between 7.99 and 17.44 kcal/mol) because these have macrocyclic cores that are arranged to maximize intramolecular hydrogen bonding interactions. Three dications were also considered (Table 6) but only the most stable form was aromatic. As these structures only differ by the placement of a single hydrogen atom, they have been designated to show the position of this atom. Two of the tautomers, **BCC-c-5H**$^{2+}$ and **BCC-c-10H**$^{2+}$, have interrupted conjugation due to the presence of methylene bridges. The favored aromatic tautomer, **BCC-c-21H**$^{2+}$, gave an NICS(0) value of −11.96 and produced large negative NICS values for rings *a*, *b*, *d*, and *e* as well. This indicates that the macrocycle again favors a 23-atom 22π electron pathway, as shown in structure **33** (Figure 13). The AICD plot also clearly demonstrates the presence of this conjugation pathway (Figure 16). The presence of an electron-withdrawing formyl unit on the benzo component would destabilize the dication and this explains why diprotonation of carbachlorins **27b,c** was not favored.

■ CONCLUSIONS

Carbachlorins are an important class of porphyrin analogues that have similar electronic properties to tetrapyrrolic chlorins while possessing improved stability toward oxidation. To expand our knowledge in this area, new families of carbachlorins have been synthesized. The *tert*-butyl ester protective groups of a dihydrodipyrrin-aldehyde and a pyrrolylmethylazulene-aldehyde were cleaved with TFA, and following dilution with acetic acid and further acidification with HI, cross-condensation produced monoprotonated azulichlorins. Azulichlorin monocations possess macrocyclic aromaticity and their UV−vis spectra give strong Soret bands. The free-base forms of azulichlorins are relatively unstable compared to the protonated species and they slowly oxidize over time to give impure carbachlorins. Proton NMR studies on the mono and diprotonated forms of azulichlorins indicated that diprotonation reduced the diatropic characteristics.

DOI: 10.1021/acs.joc.9b01578
J. Org. Chem. 2019, 84, 11649−11664

Table 5. Calculated Relative Energies (kcal/mol) and NICS Values (ppm) for Tautomers of Benzocarbachlorin Monocations

	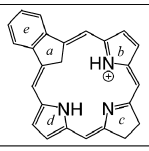	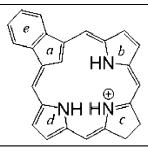	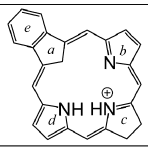	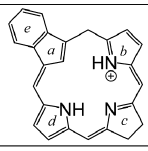	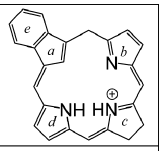
Molecule	**BCC-c-21,22,24H$^+$**	**BCC-c-22,23,24H$^+$**	**BCC-c-21,22,23H$^+$**	**BCC-c-5,22,24H$^+$**	**BCC-c-5,23,24H$^+$**
ΔG (298 K)	0.00	+8.97	+12.61	+15.61	+28.75
ΔE (B3LYP/ **M06-2X**/ B3LYP-D3)	(0.00/ **0.00**/ 0.00)	(+8.27/ **+4.78**/ +8.07)	(+12.82/ **+12.11**/ +12.88)	(+16.74/ **+16.08**/ +17.44)	(+29.76/ **+27.51**/ +30.64)
NICS(0)/NICS(1)$_{zz}$	-13.08/-31.57	-7.91/-18.54	-10.14/-23.83	-3.37/-6.46	-2.76/-5.29
NICS(*a*)/NICS(1*a*)$_{zz}$	-15.48/-44.07	+3.51/+4.30	-11.80/-34.73	+6.41/+10.44	+5.65/+10.09
NICS(*b*)/NICS(1*b*)$_{zz}$	-13.18/-33.69	-12.61/-24.82	+1.21/-5.10	-10.48/-23.24	+1.88/-3.33
NICS(*c*)/NICS(1*c*)$_{zz}$	+8.24/+14.84	+3.71/+6.12	+5.65/+13.51	+3.27/+4,21	+1.81/+5.34
NICS(*d*)/NICS(1*d*)$_{zz}$	-13.18/-33.71	-12.65/-24.85	-14.79/-31.13	-8.37/-19.99	-10.82/-22.27
NICS(*e*)/NICS(1*e*)$_{zz}$	-10.45/-33.60	-6.63/-23.18	-9.10/-30.50	-5.83/-20.19	-6.15/-21.35
	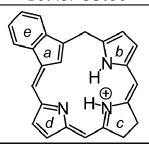	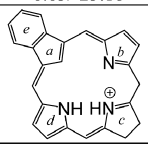	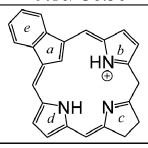	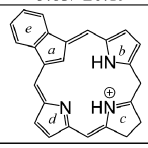	
Molecule	**BCC-c-5,22,23H$^+$**	**BCC-c-10,23,24H$^+$**	**BCC-c-10,22,24H$^+$**	**BCC-c-10,22,23H$^+$**	
ΔG (298 K)	+27.45	+29.72	+11.70	+32.52	
ΔE (B3LYP/ **M06-2X**/ B3LYP-D3)	(+28.29/ **+25.25**/ +29.12)	(+30.53/ **+25.23**/ +31.59)	(+12.54/ **+7.99**/ +13.30)	(+33.76/ **+27.37**/ +34.83)	
NICS(0)/NICS(1)$_{zz}$	-1.30/-0.22	-0.10/+1.60	+0.19/+2.30	+2.76/+10.03	
NICS(*a*)/NICS(1*a*)$_{zz}$	+10.80/+19.78	+2.95/+4.86	+0.41/-0.24	+0.92/-3.65	
NICS(*b*)/NICS(1*b*)$_{zz}$	-12.00/-29.35	-4.01/-14.99	-10.11/-21.82	-10.33/-20.92	
NICS(*c*)/NICS(1*c*)$_{zz}$	+0.29/+4.80	+0.47/+2.34	+1.88/+0.78	-8.64/-4.91	
NICS(*d*)/NICS(1*d*)$_{zz}$	+3.47/-0.17	-10.60/-22.08	-7.50/-17.73	-2.95/-11.17	
NICS(*e*)/NICS(1*e*)$_{zz}$	-4.39/-16.32	-6.97/-23.61	-7.72/-25.43	-7.77/-24.94	

Table 6. Calculated Relative Energies (kcal/mol) and NICS Values (ppm) for Unsubstituted Benzocarbachlorin Dications

	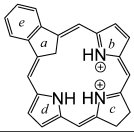	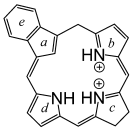	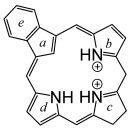
Molecule	**BCC-c-21H^{2+}**	**BCC-c-5H^{2+}**	**BCC-c-10H^{2+}**
ΔG (298 K)	0.00	+17.31	+19.32
ΔE (B3LYP/ **M06-2X**/ B3LYP-D3)	(0.00/ **0.00**/ 0.00)	(+18.38/ **+18.10**/ +19.06)	(+19.69/ **+14.07**/ +20.55)
NICS(0)/NICS(1)$_{zz}$	-11.96/-27.25	-3.59/-6.21	+0.57/+4.78
NICS(*a*)/NICS(1*a*)$_{zz}$	-14.30/-40.12	+15.78/+29.10	+2.06/+3.13
NICS(*b*)/NICS(1*b*)$_{zz}$	-13.22/-23.69	-10.68/-18.99	-9.51/-18.07
NICS(*c*)/NICS(1*c*)$_{zz}$	+7.09/+11.76	+2.08/+4.93	-0.33/+0.13
NICS(*d*)/NICS(1*d*)$_{zz}$	-13.23/-23.71	-5.81/-11.73	-8.15/-17.40
NICS(*e*)/NICS(1*e*)$_{zz}$	-9.58/-33.08	-0.99/-7.63	-7.37/-24.72

Oxidative ring contraction of an azulichlorin with *tert*-butyl hydroperoxide and KOH gave a novel benzocarbachlorin in 24% yield, together with an isomeric mixture of benzocarbachlorin-aldehydes in 37−46% yield. These benzocarbachlorins exhibit strongly aromatic characteristics, and the proton NMR spectra showed the internal C−H near −4.7 ppm. Protonation of benzocarbachlorin favored the formation of a dicationic species that enhanced the diatropic character due in part to the formation of a 22π electron delocalization pathway. On the other hand, addition of acid to benzocarbachlorin-aldehydes primarily resulted in the formation of monocations, indicating that the electron-withdrawing aldehyde groups decrease the basicity of the carbachlorin core.

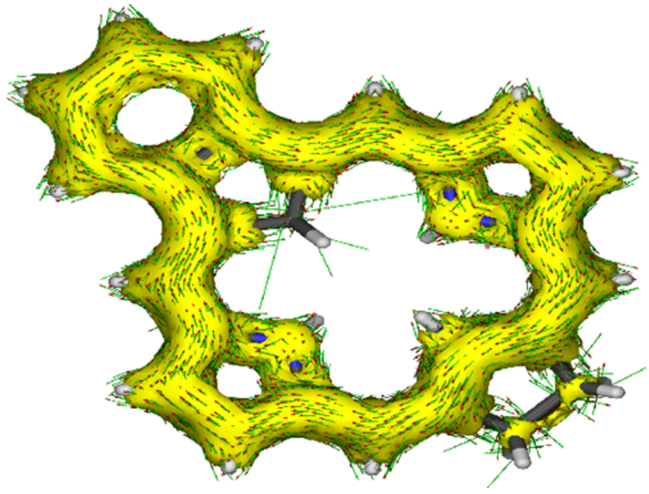

Figure 16. AICD plot (isovalue = 0.05) of benzocarbachlorin dication **BCC-c-21H^{2+}**.

■ EXPERIMENTAL SECTION

Melting points are uncorrected. NMR spectra were recorded using a 400 or 500 MHz NMR spectrometer and were run at 302 K unless otherwise indicated. ^{1}H NMR values are reported as chemical shifts δ, relative integral, multiplicity (s, singlet; d, doublet; t, triplet; q, quartet; m, multiplet; br, broad peak) and coupling constant (J). Chemical shifts are reported in parts per million (ppm) relative to $CDCl_3$ (^{1}H residual $CHCl_3$ δ 7.26, ^{13}C $CDCl_3$ triplet δ 77.23), and coupling constants were taken directly from the spectra. NMR assignments were made with the aid of ^{1}H-^{1}H COSY, HSQC, DEPT-

DOI: 10.1021/acs.joc.9b01578
J. Org. Chem. 2019, 84, 11649−11664

135, and NOE difference proton NMR spectroscopy. 2D experiments were performed by using standard software. High-resolution mass spectra (HRMS) were obtained by using a double focusing magnetic sector instrument. ^{1}H and ^{13}C NMR spectra for all new compounds are reported in the Supporting Information.

***tert*-Butyl *E*-5-(4,4-Dimethyl-5-oxo-3,4-dihydro-furan-2-ylidene)-3-ethyl-4-methyl-1*H*-pyrrole-2-carboxylate (17).** A solution of iodopyrrole **15**[52] (4.00 g, 11.9 mmol), alkyne carboxylic acid **16** (2.30 g, 18.2 mmol), benzyltriethylammonium chloride (4.46 g, 14.0 mmol), and triethylamine (29 mL) in acetonitrile (146 mL) was purged with nitrogen for 10 min and then treated with $Pd(PPh_3)_4$ (1.42 g, 1.1 mmol). The resulting mixture was heated under reflux for 17 h. At the end of this period, the solvent was removed under reduced pressure, and the residue was partitioned between dichloromethane and water. The organic layer was washed with water, dried over magnesium sulfate, filtered, and evaporated under reduced pressure. The residue was purified by flash chromatography on silica gel eluting with 5% ethyl acetate/hexanes to give lactone **17** (3.45 g, 10.3 mmol, 87%) as a colorless crystalline solid, mp 128−129 °C. ^{1}H NMR (500 MHz, $CDCl_3$): δ 1.06 (3H, t, J = 7.6 Hz, CH_2CH_3), 1.35 (6H, s, *gem*-diMe), 1.58 (9H, s, *t*-Bu), 2.24 (3H, s, pyrrole-CH_3), 2.42 (2H, q, J = 7.6 Hz, CH_2CH_3), 2.97 (2H, d, J = 2.1 Hz, lactone-CH_2), 6.21 (1H, t, J = 2.1 Hz, bridge-CH), 8.33 (1H, br s, NH). ^{13}C{^{1}H} NMR (125 MHz, $CDCl_3$): δ 10.5 (pyrrole-Me), 15.7 (CH_2CH_3), 17.5 (CH_2CH_3), 25.4 (*gem*-diMe), 28.7 (*t*-Bu), 40.3 (CMe_2), 40.6 (lactone-CH_2), 81.0 ($OCMe_3$), 97.1 (bridge-CH), 120.8, 125.7, 125.9, 127.4, 147.5, 161.8 (ester-C═O), 179.2 (lactone-C═O). EIMS: m/z (rel. int.) 333 (23, M^+), 277 (100, $[M - C_4H_8]^+$), 262 (10, $[M - C_4H_8 - CH_3]^+$), 260 (10, $[M - C_4H_9O]^+$), 233 (9, $[M - C_4H_8 - CO_2]^+$), 193 (86). HRMS (EI): m/z calcd for $C_{19}H_{27}NO_4$, 333.1940; found, 333.1946.

***tert*-Butyl *E*-5-(4,4-Dimethyl-5-methylene-3,4-dihydro-furan-2-ylidene)-4-ethyl-3-methyl-1*H*-pyrrole-2-carboxylate (18).** A suspension of titanocene dichloride (1.47 g; 5.97 mmol) in anhydrous toluene (16 mL) was treated with 8.2 mL (13.1 mmol) of 1.6 M methyllithium in diethyl ether over 5 min at 0 °C. After stirring the solution for 1 h at 0 °C, the reaction was quenched with 14 mL of 6% aqueous ammonium chloride solution. The organic layer was separated and washed sequentially with water and brine, dried over sodium sulfate, and filtered to give an orange solution of dimethyl titanocene. Lactone **17** (0.420 g, 1.26 mmol) and titanocene dichloride (19 mg; 0.076 mmol) were added to the solution, and the mixture was refluxed for 24 h. The flask was cooled to room temperature, and methanol (1.5 mL), sodium bicarbonate (63 mg), and water (15 μL) were added. The resulting solution was stirred for 12 h at 40 °C and filtered through a pad of Celite, and the residue was further washed with hexanes. If necessary, the filtrate was filtered a second time, and the solvents were then removed under reduced pressure. The resulting oil was purified by flash chromatography on silica gel eluting with 20% dichloromethane/hexanes containing 1% triethylamine. Following evaporation of the solvents, the enol ether (0.32 g, 0.96 mmol, 76%) was obtained as yellow crystals, mp 86−90 °C. ^{1}H NMR (500 MHz, $CDCl_3$): δ 1.05 (3H, t, J = 7.5 Hz, CH_2CH_3), 1.27 (6H, s, *gem*-diMe), 1.57 (9H, s, *t*-Bu), 2.27 (3H, s, pyrrole-CH_3), 2.44 (2H, q, J = 7.5 Hz, CH_2CH_3), 2.72 (2H, d, J = 1.9 Hz, CH_2CMe_2), 4.02 (1H, d, J = 2.4 Hz), 4.40 (1H, d, J = 2.4 Hz) (═CH_2), 5.95 (1H, t, J = 1.9 Hz, bridge-CH), 8.30 (1H, br s, NH). ^{13}C{^{1}H} NMR (125 MHz, $CDCl_3$): δ 10.6 (pyrrole-Me), 15.7 (CH_2CH_3), 17.5 (CH_2CH_3), 28.0 (*gem*-diMe), 28.8 (*t*-Bu), 40.6 (CMe_2), 42.5 (CH_2CMe_2), 80.6 ($OCMe_3$), 81.0 (═CH_2), 92.0 (bridge-CH), 119.6, 125.7, 125.8, 128.1, 153.8, 161.8, 169.1. EIMS: m/z (rel. int.) 331 (22, M^+), 275 (100, $[M - C_4H_8]^+$), 260 (24, $[M - C_4H_8 - CH_3]^+$), 242 (23). HRMS (EI): m/z calcd for $C_{20}H_{29}NO_3$, 331.2147; found 331.2151.

***tert*-Butyl *Z*-4-Ethyl-3-methyl-5-(4,4,5-trimethyl-3,4-dihydropyrrol-2-ylidene)-1*H*-pyrrole-2-carboxylate (14).** . A solution of enol ether **18** (1.02 g, 3.08 mmol) in DMF (24 mL) was treated with 210 μL (0.13 mmol) of 6 M HCl and stirred at room temperature until the formation of diketone **19** was complete (ca. 1 h; monitored by TLC, R_f on silica with 20% ethyl acetate/hexanes of 0.20). The reaction was then treated with ammonium acetate (8.0 g, 10.2 mmol) and triethylamine (14 mL, 10.2 mmol), and the resulting solution was heated at 55 °C until product formation was complete by TLC (ca. 6 h; R_f on silica with 20% ethyl acetate/hexanes of 0.55). The mixture was diluted with 10% KH_2PO_4 (24 mL) and extracted with dichloromethane (3 × 25 mL). The combined organic extracts were washed sequentially with water (2 × 50 mL) and brine, dried over sodium sulfate, filtered, and concentrated under reduced pressure. The resulting oil was purified by flash chromatography on silica gel, eluting with 10% ethyl acetate/hexanes to give the dihydrodipyrrin (0.71 g, 2.15 mmol, 70%) as a red crystalline solid, mp 118−120 °C. ^{1}H NMR (500 MHz, $CDCl_3$): δ 1.07 (3H, t, J = 7.5 Hz, CH_2CH_3), 1.18 (6H, s, *gem*-diMe), 1.57 (9H, s, *t*-Bu), 2.14 (3H, s, imine-CH_3), 2.27 (3H, s, pyrrole-CH_3), 2.44 (2H, q, J = 7.5 Hz, CH_2CH_3), 2.58 (2H, d, J = 1.8 Hz, pyrroline-CH_2), 5.82 (1H, br t, bridge-CH), 11.08 (1H, br s, NH). ^{13}C{^{1}H} NMR (125 MHz, $CDCl_3$): δ 10.3 (pyrrole-Me), 15.9 (imine-Me), 16.3 (CH_2CH_3), 17.3 (CH_2CH_3), 25.8 (*gem*-diMe), 28.7 (*t*-Bu), 44.7 (pyrroline-CH_2), 48.5 (CMe_2), 79.7 ($OCMe_3$), 103.4 (bridge-CH), 119.8, 125.2, 125.5, 130.1, 151.5, 161.3, 188.0. EIMS: m/z (rel. int.) 330 (28, M^+), 274 (100, $[M - C_4H_8]^+$), 259 (18, $[M - C_4H_8 - CH_3]^+$), 241 (26). HRMS (EI): m/z calcd for $C_{20}H_{30}N_2O_2$, 330.2307; found, 330.2310.

***tert*-Butyl *Z*-5-(5-Formyl-3,4-dihydro-4,4-dimethylpyrrol-2-ylidene)-4-ethyl-3-methyl-1*H*-pyrrole-2-carboxylate (20).** Selenium dioxide (289 mg, 2.60 mmol) was added to a solution of dihydrodipyrrin **14** (717 mg, 2.17 mmol) in DMF (20 mL) and pyridine (210 μL, 2.60 mmol) and stirred at room temperature for 5 h. The mixture was then heated to 80 °C for 15 min, cooled to room temperature, filtered, and poured into water. The mixture was extracted with dichloromethane (3 × 10 mL), and the combined organic extracts were washed sequentially with saturated aqueous sodium bicarbonate and brine, dried over Na_2SO_4, and filtered, and the solvent was removed under reduced pressure. The resulting oil was purified by flash chromatography on silica gel eluting with toluene to give the aldehyde (346 mg, 1.00 mmol, 46%) as an orange crystalline solid, mp 119−121 °C. ^{1}H NMR (500 MHz, $CDCl_3$): δ 1.10 (3H, t, J = 7.6 Hz, CH_2CH_3), 1.36 (6H, s, *gem*-diMe), 1.58 (9H, s, *t*-Bu), 2.28 (3H, s, pyrrole-CH_3), 2.50 (2H, q, J = 7.6 Hz, CH_2CH_3), 2.74 (2H, d, J = 1.8 Hz, pyrroline-CH_2), 6.24 (1H, t, J = 1.8 Hz, bridge-CH), 9.92 (1H, s, CHO), 10.78 (1H, br s, NH). ^{13}C{^{1}H} NMR (125 MHz, $CDCl_3$): δ 10.2 (pyrrole-Me), 16.4 (CH_2CH_3), 17.4 (CH_2CH_3), 25.8 (*gem*-diMe), 28.7 (*t*-Bu), 46.5 (CMe_2), 46.6 (pyrroline-CH_2), 80.6 ($OCMe_3$), 113.1 (bridge-CH), 122.9, 125.6, 129.1, 129.4, 150.9, 160.9, 177.8, 190.3 (CHO). EIMS: m/z (rel. int.) 344 (25, M^+), 288 (27, $[M - C_4H_8]^+$), 273 (100, $[M - C_4H_8 - CH_3]^+$), 255 (45), 241 (14). HRMS (EI): m/z calcd for $C_{20}H_{28}N_2O_3$, 344.2100; found, 344.2096.

***tert*-Butyl 5-(6-*tert*-Butyl-1-azulenylmethyl)-4-ethyl-3-methylpyrrole-2-carboxylate (23b).** *tert*-Butylazulene (489 mg, 2.66 mmol) and *tert*-butyl 5-acetoxymethyl-4-ethyl-3-methylpyrrole-2-carboxylate[53] (**22**, 740 mg, 2.63 mmol) were dissolved in 2-propanol (40 mL) and acetic acid (4 mL), and the solution was refluxed with stirring under nitrogen for 16 h. The solvent was evaporated under reduced pressure, and the residue was purified by column chromatography on silica, eluting initially with 40% dichloromethane/hexanes and then with gradually increased proportions of CH_2Cl_2. Initially, a blue fraction corresponding to unreacted 6-*tert*-butylazulene was collected, followed by a major blue band for the title compound. A third blue band corresponding to an azulitripyrrane byproduct was also collected. Following evaporation of the solvent, the azulidipyrrane (680 mg, 1.68 mmol, 63%) was obtained as a dark-blue solid, mp 124−126 °C. A sample was recrystallized from ethanol/water to give dark-blue crystals, mp 125−126 °C. ^{1}H NMR (500 MHz, $CDCl_3$): δ 1.13 (3H, t, J = 7.5 Hz, CH_2CH_3), 1.45 (9H, s), 1.48 (9H, s) (2× *t*-Bu), 2.28 (3H, s, pyrrole-CH_3), 2.53 (2H, q, J = 7.5 Hz, CH_2CH_3), 4.34 (2H, s, bridge-CH_2), 7.25 (1H, d, J = 3.8 Hz, 2-H), 7.29−7.31 (1H, m), 7.31−7.33 (1H, m) (5,7-H), 7.62 (1H, d, J = 3.8 Hz), 8.13 (1H, br s, NH), 8.18 (1H, d, J = 10.6 Hz), 8.24 (1H, d, J = 10.5 Hz) (4,8-H). ^{13}C{^{1}H} NMR ($CDCl_3$): δ 10.7 (pyrrole-Me), 15.7 (CH_2CH_3), 17.6 (CH_2CH_3), 24.4 (bridge-CH_2), 28.7 (ester *t*-Bu),

DOI: 10.1021/acs.joc.9b01578
J. Org. Chem. 2019, 84, 11649−11664

32.1 (azulene-*t*-Bu), 38.8 (6-CMe_3), 80.1 ($OCMe_3$), 116.7 (2-CH), 118.6, 120.6 (5- or 7-CH), 121.0 (5- or 7-CH), 123.3, 125.0, 126.0, 132.1, 132.6 (4- or 8-CH), 135.1, 136.1 (4- or 8-CH), 137.0 (3-CH), 139.9, 161.5, 161.8. HRMS (EI) calcd for $C_{27}H_{35}NO_2$, 405.2668; found, 405.2661.

3(5-*tert*-Butoxycarbonyl-3-ethyl-4-methyl-2-pyrrolylmethyl)-azulene-1-carbaldehyde (21a). Phosphorus oxychloride (0.6 mL) was added dropwise to DMF (1 mL) in a 250 mL round-bottom flask while the temperature was maintained between 10 and 20 °C with the aid of an ice bath. The mixture was allowed to stand for 15 min at room temperature. The Vilsmeier reagent was diluted with 32 mL of CH_2Cl_2, followed by the addition of 4.0 g of potassium carbonate. Azulidipyrrane **23a**[40] (600 mg, 1.72 mmol) in dichloromethane (40 mL) was added dropwise over 10 min. The resulting mixture was stirred at room temperature for 1 h, and then a solution of sodium acetate trihydrate (22.0 g) in water (40 mL) was added. The resulting biphasic mixture was stirred under reflux for 15 min. The mixture was cooled, the organic layer was separated, and the aqueous phase was extracted with chloroform. The combined organic layers were dried over sodium sulfate and evaporated under reduced pressure. The residue was recrystallized from ethanol to give pyrrolylmethylazulene-aldehyde **21a** (450 mg, 1.19 mmol, 69%) as a dark-purple powder, mp 147−149 °C. ^{1}H NMR (500 MHz, $CDCl_3$): δ 1.08 (3H, t, J = 7.5 Hz, CH_2CH_3), 1.50 (9H, s, *t*-Bu), 2.28 (3H, s, pyrrole-Me), 2.49 (2H, q, J = 7.5 Hz, CH_2CH_3), 4.32 (2H, s, bridge-CH_2), 7.51 (1H, t, J = 9.8 Hz, 7-H), 7.62 (1H, t, J = 9.8 Hz, 5-H), 7.86 (1H, t, J = 9.9 Hz, 6-H), 8.03 (1H, s, 2-H), 8.26 (1H, br s, NH), 8.41 (1H, d, J = 9.8 Hz, 8-H), 9.56 (1H, d, J = 9.7 Hz, 4-H), 10.31 (1H, s, CHO). ^{13}C{^{1}H} NMR (125 MHz, $CDCl_3$): δ 10.7 (pyrrole-Me), 15.7 (CH_2CH_3), 17.6 (CH_2CH_3), 24.4 (bridge-CH_2), 28.7 (*t*-Bu), 80.5 ($OCMe_3$), 119.2, 124.0, 124.8, 126.0, 127.4, 128.0 (7-CH), 129.9 (5-CH), 130.2, 136.0 (8-CH), 137.8 (4-CH), 140.3 (6-CH), 141.5, 142.3 (2-CH), 142.5, 161.6 (ester C═O), 186.4 (CHO). EIMS: m/z (rel. int.) 377 (20, M^+), 354 (26), 321 (14, $[M - C_4H_8]^+$), 308 (19), 277 (32), 274 (45), 273 (35), 255 (16). HRMS (EI): m/z calcd for $C_{24}H_{27}NO_3$, 377.1991; found, 377.1994.

6-*tert*-Butyl-3(5-*tert*-butoxycarbonyl-3-ethyl-4-methyl-2-pyrrolylmethyl)-azulene-1-carbaldehyde (21b). Phosphorus oxychloride (0.3 mL) was added dropwise to DMF (0.5 mL) in a 100 mL round-bottom flask while the temperature was maintained between 10 and 20 °C with the aid of an ice bath. The mixture was allowed to stand for 15 min at room temperature. The Vilsmeier reagent was diluted with 16 mL of CH_2Cl_2, followed by the addition of 2.0 g of potassium carbonate. Pyrrolylmethylazulene **23b** (300 mg, 0.74 mmol) in dichloromethane (20 mL) was added dropwise over 10 min. The resulting mixture was stirred at room temperature for 1 h, and then a solution of sodium acetate trihydrate (11.0 g) in water (20 mL) was added. The resulting biphasic mixture was stirred under reflux for 15 min. The mixture was cooled, the organic layer was separated, and the aqueous phase was extracted with chloroform. The combined organic layers were dried over sodium sulfate and evaporated under reduced pressure. The residue was recrystallized from ethanol to give the azulidipyrrin-aldehyde **21b** (220 mg, 0.51 mmol, 68%), as a dark-maroon powder, mp 198−200 °C. ^{1}H NMR (500 MHz, $CDCl_3$): δ 1.09 (3H, t, J = 7.5 Hz, CH_2CH_3), 1.48 (9H, s), 1.49 (9H, s) (2× *t*-Bu), 2.28 (3H, s, pyrrole-CH_3), 2.50 (2H, q, J = 7.5 Hz, CH_2CH_3), 4.29 (2H, s, bridge-CH_2), 7.69 (1H, dd, J = 1.9, 10.6 Hz, 7-H), 7.80 (1H, dd, J = 1.8, 10.6 Hz, 5-H), 7.96 (1H, s, 2-H), 8.21 (1H, br s, NH), 8.33 (1H, d, J = 10.6 Hz, 8-H), 9.47 (1H, d, J = 10.6 Hz, 4-H), 10.28 (1H, s, CHO). ^{13}C{^{1}H} NMR (125 MHz, $CDCl_3$): δ 10.7 (pyrrole-Me), 15.8 (CH_2CH_3), 17.6 (CH_2CH_3), 24.3 (bridge-CH_2), 28.7 (ester *t*-Bu), 32.0 (azulene *t*-Bu), 39.2 (azulene-CMe_3), 80.4 ($OCMe_3$), 119.1, 123.8, 124.6, 126.0, 126.64 (7-CH), 126.68, 127.9 (5-CH), 130.6, 135.0 (8-CH), 136.9 (4-CH), 140.4, 141.2 (2-CH), 141.4, 161.6, 165.1, 186.2 (CHO). EIMS: m/z (rel. int.) 433 (28, M^+), 377 (19, $[M - C_4H_8]^+$), 348 (12, $[M - C_4H_8 - CHO]^+$), 333 (9, $[M - C_4H_8 - CO_2]^+$), 304 (5, $[M - C_4H_8 - CO_2 - CHO]^+$), 213 (61), 165 (100). HRMS (EI): m/z calcd for $C_{28}H_{35}NO_3$, 433.2617; found, 433.2622.

8,17-Diethyl-8,12,12,12,18-tetramethyl-12,13-dihydroazuliporphyrin hydoiodide (25a.HI). Azulidipyrrane-aldehyde **21a** (40 mg, 0.106 mmol) and dihydrodipyrrin-aldehyde **20** (36.5 mg, 0.106 mmol) were dissolved in 5 mL of TFA and stirred at room temperature for 10 min in the dark. The solution was diluted with 100 mL of acetic acid, 14 drops of hydroiodic acid were added, and the mixture was stirred overnight in the dark. The solution was diluted with CH_2Cl_2 and washed with water. The organic layer was separated, dried with sodium sulfate, and evaporated under reduced pressure. The residue was purified on a silica column, eluting with CH_2Cl_2 containing 2−5% methanol. The product, which was collected as a deep green band, was further purified on a grade 3 basic alumina column, eluting with 4% methanol/dichloromethane. The green band was collected, the solvent was removed on a rotary evaporator, and the residue was dried in vacuo to give the azulichlorin (11 mg, 0.018 mmol, 17%) as a dark-green powder, mp >300 °C. UV−vis (1% $Et_3N/CHCl_3$): λ_{max}/nm (log ε) 348 (4.55), 391 (sh, 4.55), 410 (sh, 4.59), 439 (4.64), 483 (sh, 4.64). UV−vis ($CHCl_3$): λ_{max}/nm ($\log_{10}$ ε) 368 (4.57), 408 (sh, 4.62), 418 (sh, 4.65), 444 (4.92), 497 (sh, 4.22), 615 (4.30), 657 (4.27). UV−vis (5% TFA/$CHCl_3$): λ_{max}/nm (log ε) 345 (4.57), 457 (5.00), 505 (4.37), 605 (sh, 4.30), 645 (4.41). ^{1}H NMR (500 MHz, $CDCl_3$): δ −2.11 (1H, s, 21-H), −0.41 (1H, br s), −0.28 (1H, br s) (2× NH), 1.53 (3H, t, J = 7.8 Hz, 7-CH_2CH_3), 1.60 (3H, t, J = 7.7 Hz, 17-CH_2CH_3), 1.71 (6H, s, *gem*-diMe), 2.98 (3H, s, 8-CH_3), 3.23 (3H, s, 18-CH_3), 3.34 (2H, q, J = 7.7 Hz, 17-CH_2), 3.79 (2H, q, J = 7.8 Hz, 7-CH_2), 3.82 (2H, s, 13-CH_2), 7.51 (1H, s, 10-H), 7.58 (1H, s, 15-H), 8.06 (1H, t, J = 9.6 Hz, 2^3-H), 8.23 (1H, t, J = 9.6 Hz, 3^2-H), 8.26 (1H, t, J = 9.6 Hz, 2^2-H), 9.22 (1H, s, 20-H), 9.28 (1H, s, 5-H), 10.08 (1H, d, J = 9.6 Hz, 3^1-H), 10.14 (1H, d, J = 9.7 Hz, 2^1-H). ^{13}C{^{1}H} NMR (125 MHz, $CDCl_3$): δ 10.5 (8-Me), 11.7 (18-Me), 16.2 (7- CH_2CH_3), 16.9 (17- CH_2CH_3), 18.7 (7-CH_2), 19.6 (17-CH_2), 30.5 (*gem*-diMe), 46.4 (CMe_2), 52.0 (13-CH_2), 90.3 (10-CH), 92.5 (15-CH), 105.2 (5- or 20-CH), 105.4 (5- or 20-CH), 116.9 (21-CH), 125.1, 125.2, 129.7, 135.7, 136.3, 136.44, 136.49, 136.8, 140.0 (3^1-CH), 140.4 (2^1-CH), 140.9, 144.2 (2^3-CH), 146.3, 146.4, 147.3, 147.4, 148.9, 171.3, 182.9. ^{1}H NMR (500 MHz, TFA/$CDCl_3$, dication $\mathbf{25}H_2^{2+}$): δ 1.26 (1H, s, NH), 1.43 (3H, t, J = 7.7 Hz, 17-CH_2CH_3), 1.51 (3H, t, J = 7.7 Hz, 7-CH_2CH_3), 1.82 (6H, s, *gem*-diMe), 2.24 (1H, s, 21-H), 2.79 (3H, s, 8-CH_3), 2.99 (3H, s, 18-CH_3), 3.19 (2H, q, J = 7.7 Hz, 17-CH_2), 3.43 (2H, q, J = 7.7 Hz, 7-CH_2), 3.98 (2H, s, 13-CH_2), 5.40 (1H, br s), 5.41 (1H, br s) (2× NH), 7.34 (1H, s, 10-H), 7.48 (1H, s, 15-H), 8.19−8.30 (3H, m, $2,^2 2,^3 3^2$-H), 9.238 (1H, s), 9.241 (1H, s) (5,20-H), 9.42 (1H, d, J = 9.4 Hz), 9.43 (1H, d, J = 9.5 Hz) ($2,^1 3^1$-H). ^{13}C{^{1}H} NMR (125 MHz, TFA/$CDCl_3$, dication $\mathbf{25}H_2^{2+}$): δ 10.4, 11.1, 15.1, 15.9, 18.6, 19.5, 29.5, 44.9, 47.6, 89.1, 91.0, 114.19, 114.22, 126.2, 126.3, 131.4, 132.2, 137.6, 137.7, 138.57, 138.62, 139.0, 139.4, 140.6, 144.2, 145.5, 149.74, 149.77, 150.5, 154.1, 155.2, 155.3, 165.9. HRMS (ESI): m/z $[M + H]^+$ calcd for $C_{34}H_{36}N_3$, 486.2909; found, 486.2911.

2^3-*tert*-Butyl-8,17-diethyl-8,12,12,12,18-tetramethyl-12,13-dihydroazuliporphyrin hydoiodide (25b.HI). *tert*-Butylazulidipyrrane-aldehyde **21b** (42 mg, 0.096 mmol) and **20** (36 mg, 0.10 mmol) were reacted under the foregoing conditions. The crude product was purified on silica column, eluting with 2−5% methanol/dichloromethane, and then it was purified on a grade 3 basic alumina column, eluting with 4% methanol/dichloromethane. The resulting major green band was evaporated under reduced pressure, and the residue was dried overnight in a vacuum desiccator to give the *tert*-butyl azulichlorin (10 mg, 0.015 mmol, 15%) as a dark-green powder, mp >300 °C. UV−vis (1% $Et_3N/CHCl_3$): λ_{max}/nm (log ε) 348 (4.50), 368 (4.50), 444 (4.59), 595 (sh, 4.07). UV−vis ($CHCl_3$): λ_{max}/nm (log ε) 366 (4.54), 407 (sh, 4.51), 418 (sh, 4.57), 445 (4.87), 498 (4.22), 615 (4.29), 657 (4.27). UV−vis (5% TFA/$CHCl_3$): λ_{max}/nm (log ε) 341 (4.55), 459 (4.95), 507 (sh, 4.32), 602 (sh, 4.29), 643 (4.44). ^{1}H NMR (500 MHz, $CDCl_3$): δ −1.46 (1H, s, 21-H), 0.13 (1H, br s), 0.21 (1H, br s) (2× NH), 1.54 (3H, t, J = 7.7 Hz, CH_2CH_3), 1.63 (9H, s, *t*-Bu), 1.65 (3H, t, J = 7.7 Hz, CH_2CH_3), 1.80 (6H, s, *gem*-diMe), 3.02 (3H, s, 8-CH_3), 3.30 (3H, s, 18-CH_3), 3.39 (2H, q, J = 7.7 Hz), 3.81 (2H, q, J = 7.7 Hz) (2× CH_2CH_3), 4.04 (2H, s, 13-CH_2), 7.72 (1H, s, 10-H), 7.83 (1H, s, 15-H), 8.54 (1H,

DOI: 10.1021/acs.joc.9b01578
J. Org. Chem. 2019, 84, 11649−11664

dd, J = 1.7, 10.5 Hz), 8.58 (1H, dd, J = 1.7, 10.5 Hz) (2,^{2}3^2-H), 9.60 (1H, s), 9.65 (1H, s) (5,20-H), 10.16 (1H, d, J = 10.5 Hz), 10.30 (1H, d, J = 10.6 Hz) (2,^{1}3^1-H). ^{13}C{^{1}H} NMR (125 MHz, $CDCl_3$): δ 10.6, 11.9, 16.2, 17.0, 18.7, 19.7, 30.6, 32.0, 40.2, 46.6, 52.2, 90.5, 92.7, 105.3, 105.6, 116.8, 125.5, 125.8, 129.8, 134.8, 135.1, 135.7, 136.6, 137.0, 139.1, 139.6, 140.7, 146.0, 146.1, 147.13, 147.15, 148.7, 170.3, 171.2, 182.7. ^{1}H NMR (500 MHz, TFA/$CDCl_3$, dication **25b**H_2^{2+}): δ 1.26 (1H, s), 1.44 (3H, t, J = 7.6 Hz), 1.52 (3H, t, J = 7.7 Hz), 1.63 (9H, s), 1.83 (6H, s), 1.85 (1H, br s), 2.80 (3H, s), 3.00 (3H, s), 3.21 (2H, q, J = 7.6 Hz), 3.45 (2H, q, J = 7.7 Hz), 4.01 (2H, s), 5.11 (1H, br s), 5.12 (1H, br s), 7.40 (1H, s), 7.54 (1H, s), 8.43 (2H, d, J = 10.5 Hz), 9.29 (2H, s), 9.39−9.42 (2H, m). HRMS (ESI): m/z [M + H]$^+$ calcd for $C_{38}H_{44}N_3$, 542.3535; found, 542.3536.

8,17-Diethyl-8,12,12,12,18-tetramethyl-12,13-dihydrobenzo[*b*]carbaporphyrin (27a). Potassium hydroxide (100 mg) in 12 mL of methanol and a solution of *tert*-butyl hydroperoxide in decane (5 M, 20 μL) were added to a solution of azulichlorin **25a**.HI (10.0 mg, 0.016 mmol) in dichloromethane (12 mL), and the resulting mixture was stirred under nitrogen in the dark for 40 min. The solution was diluted with chloroform, washed with water (two times), dried over sodium sulfate, and evaporated under reduced pressure. The residues were chromatographed on a grade 3 alumina column, eluting initially with 30% dichloromethane/hexanes. An orange band was collected, the solvent was evaporated, and the residue was recrystallized from chloroform/hexanes to give a yellow-brown powder (1.9 mg, 0.0040 mmol, 24%) corresponding to benzocarbachlorin **27a**, mp >300 °C. UV−vis (1% $Et_3N/CHCl_3$): λ_{max}/nm (log ε) 344 (4.18), 363 (4.18), 414 (4.64), 430 (4.64), 507 (3.81), 515 (3.82), 540 (sh, 3.50), 622 (3.30), 653 (sh, 3.38), 684 (4.29). UV−vis (5% TFA/$CHCl_3$; dication **27a**H_2^{2+}): λ_{max}/nm (log ε) 343 (sh, 4.09), 361 (4.35), 404 (4.80), 484 (sh, 3.71), 557 (3.46), 606 (3.27), 762 (sh, 3.69), 800 (4.44). ^{1}H NMR (500 MHz, $CDCl_3$): δ −4.64 (1H, s, 21-H), −2.63 (1H, br s), −2.58 (1H, br s) (2× NH), 1.71 (3H, t, J = 7.7 Hz, 17- CH_2CH_3), 1.76 (3H, t, J = 7.7 Hz, 7-CH_2CH_3), 2.01 (6H, s, *gem*-diMe), 3.34 (3H, s, 8-CH_3), 3.44 (3H, s, 18-CH_3), 3.76 (2H, q, J = 7.7 Hz, 17-CH_2), 3.92 (2H, q, J = 7.7 Hz, 7-CH_2), 4.51 (2H, br s, 13-CH_2), 7.65−7.68 (2H, m, 2,^{2}3^2-H), 8.47 (1H, s, 10-H), 8.59 (1H, s, 15-H), 8.68−8.73 (2H, m, 2,^{1}3^1-H), 9.72 (1H, s, 20-H), 9.76 (1H, s, 5-H). ^{13}C{^{1}H} NMR (125 MHz, $CDCl_3$): δ 10.9 (8-Me), 11.4 (18-Me), 17.1 (17-CH_2CH_3), 17.4 (7-CH_2CH_3), 19.2 (17-CH_2), 19.8 (7-CH_2), 31.5 (*gem*-diMe), 46.4 (CMe_2), 52.7 (13-CH_2), 90.2 (10-CH), 92.1 (15-CH), 101.3 (20-CH), 101.6 (5-CH), 111.4 (21-CH), 120.0 (2^1- and 3^1-CH), 125.43, 125.48 (2,^{2}3^2-CH), 129.8, 129.9, 130.0, 131.7, 132.9, 133.0, 133.4, 137.6, 138.8, 139.8, 140.37, 140.42, 161.5, 173.1. ^{1}H NMR (500 MHz, TFA/$CDCl_3$, dication **27a**H_2^{2+}): δ −6.77 (2H, s, 21-CH_2), −3.45 (1H, br s), −3.42 (1H, br s) (2× NH), 1.83 (3H, t, J = 7.7 Hz), 1.90 (3H, t, J = 7.7 Hz) (2× CH_2CH_3), 2.18 (6H, s, *gem*-diMe), 3.60 (3H, s, 8-CH_3), 3.71 (3H, s, 18-CH_3), 4.02 (2H, q, J = 7.7 Hz, 17-CH_2), 4.18 (2H, q, J = 7.7 Hz, 7-CH_2), 4.88 (2H, s, 13-CH_2), 8.74−8.78 (2H, m, 2,^{2}3^2-H), 9.47 (1H, s, 10-H), 9.64 (1H, s, 15-H), 10.09−10.12 (2H, m, 2,^{1}3^1-H), 11.120 (1H, s), 11.126 (1H, s) (5,20-H). ^{13}C{^{1}H} NMR (125 MHz, TFA/$CDCl_3$, dication **27a**H_2^{2+}): δ 11.4 (8-Me), 11.7 (18-Me), 17.2 (CH_2CH_3), 17.3 (CH_2CH_3), 19.7 (17-CH_2), 20.0 (7-CH_2), 31.7 (*gem*-diMe), 32.0 (21-CH_2), 47.8 (12-C), 53.1 (13-CH_2), 101.2 (10-CH), 103.2 (15-CH), 105.8 (5- and 20-CH), 123.64, 123.70 (2,^{1}3^1-CH), 131.7, 131.8 (2,^{2}3^2-CH), 134.8, 136.1, 137.8, 138.2, 139.1, 139.6, 136.7, 142.0, 142.9, 143.6, 143.8, 166.6, 178.0. HRMS (ESI): m/z [M + H]$^+$ calcd for $C_{33}H_{36}N_3$, 474.2909; found, 474.2908.

Benzocarbachlorin Carbaldehydes 27b and 27c. A second major band was collected (3.0−3.8 mg, 0.0060−0.0076 mmol, 37−46%) corresponding to a 50/50 mixture of benzocarbachlorin-aldehydes, mp >300 °C. UV−vis (1% $Et_3N/CHCl_3$): λ_{max}/nm (log ε) 342 (4.51), 442 (5.02), 530 (sh, 3.91), 557 (4.10), 616 (3.66), 646 (3.45), 676 (4.45). UV−vis (0.5% TFA/$CHCl_3$; monocations **27b,c**H^+): λ_{max}/nm (log ε) 339 (4.38), 450 (4.93), 535 (3.89), 575 (sh, 3.49), 645 (sh, 3.53), 677 (sh, 3.89), 707 (4.59). ^{1}H NMR (500 MHz, $CDCl_3$): δ −4.70 (s), −4.69 (s) (1H), −2.74 (1H, br s), −2.69 (s), −2.67 (br s) (1H), 1.67−1.74 (6H, m), 2.02 (6H, s), 3.29 (s), 3.30 (s) (3H), 3.34 (3H, s), 3.67−3.72 (2H, m), 3.82 (2H, q, J = 7.5 Hz), 4.48 (2H, s), 7.97−8.01 (1H, m), 8.43 (1H, s), 8.52 (1H, s), 8.53−8.58 (1H, m), 8.97 (s), 8.99 (s) (1H), 9.46 (s), 9.51 (s), 9.52 (s), 9.55 (s) (2H), 10.28 (1H, s). ^{13}C{^{1}H} NMR (125 MHz, $CDCl_3$): δ 10.84, 10.86, 11.3, 17.0, 17.36, 17.41, 19.2, 19.69, 19.73, 31.5, 46.5, 52.7, 90.27, 90.31, 92.20, 92.24, 101.5, 101.6, 101.8, 102.0, 112.9 (21-CH), 119.81, 119.85, 120.8, 121.0, 126.49, 126.52, 127.4, 127.48, 127.53, 127.6, 128.0, 128.1, 131.7, 131.8, 133.0, 133.1, 133.58, 133.63, 133.73, 133.78, 133.81, 133.86, 138.55, 133.59, 139.8, 140.6, 140.8, 144.86, 144.91, 162.70, 162.74, 174.24, 174.26, 193.16, 193.19. ^{1}H NMR (500 MHz, TFA/$CDCl_3$, monocations **27b,c**H^+): δ −2.03 (1H, s), 1.45−1.48 (3H, 2 overlapping triplets), 1.50−1.54 (3H, 2 overlapping triplets), 1.95 (6H, s), 3.02 (1H, br s), 3.17 (br s), 3.18 (br s) (1H), 3.44−3.49 (2H, m), 3.62−3.70 (2H, m), 4.32 (2H, s), 7.96 (1H, s), 8.08 (1H, s), 8.15−8.17 (1H, br d), 8.56−8.59 (1H, m), 9.02 (s), 9.04 (s) (1H), 9.61 (1H, s), 9.66 (s), 9.67 (s) (1H), 10.20 (1H, s). HRMS (ESI): m/z [M + H]$^+$ calcd for $C_{34}H_{36}N_3O$, 502.2858; found, 502.2861.

Computational Studies. All calculations were performed using Gaussian 09 Rev. D.01 running on a Linux-based computer.[54] Energy minimization and frequency calculations of the porphyrinoid systems were performed at the density functional theory (DFT) level of theory with the B3LYP functional and the 6-311++G(d,p) triple-ζ basis set.[55−58] Single-point energy calculations were performed on the minimized structures using both the B3LYP-D3[59] and M062-X[60] functionals with a 6−311++G(d,p) triple-ζ basis set. The resulting Cartesian coordinates of the molecules can be found in the Supporting Information.

Two types of NMR calculations were performed: the GIAO method with the B3LYP functional and a 6-31 + G(d,p) basis set was used to obtain NICS values,[61] and CGST with the B3 functional and a 6-31 + G(d,p) basis set to obtain AICD plots.[62] NICS(0) was calculated at the mean position of all four heavy atoms in the middle of the macrocycle. NICS(a), NICS(b), NICS(c), NICS(d), and NICS(e) values were obtained by applying the same method to the mean position of the heavy atoms that comprise the individual rings of each macrocycle. In addition, NICS(1)$_{zz}$, NICS(1a)$_{zz}$, NICS(1b)$_{zz}$, NICS(1c)$_{zz}$, NICS(1d)$_{zz}$, and NICS(1e)$_{zz}$ were obtained by applying the same method to ghost atoms placed 1 Å above each of the corresponding NICS(0) points and extracting the zz contribution of the magnetic tensor. AICD for all the compounds were plotted, and these plots can also be found in the Supporting Information.

■ ASSOCIATED CONTENT

Supporting Information

The Supporting Information is available free of charge on the ACS Publications website at DOI: 10.1021/acs.joc.9b01578.

Tables giving Cartesian coordinates, calculated energies, selected bond lengths, and AICD plots and selected UV−vis, ^{1}H NMR, ^{1}H-^{1}H COSY, HSQC, DEPT-135, ^{13}C{^{1}H} NMR, and mass spectra (PDF)

■ AUTHOR INFORMATION

Corresponding Author

*E-mail: tdlash@ilstu.edu.

ORCID

Timothy D. Lash: 0000-0002-0050-0385

Notes

The authors declare no competing financial interest.

■ ACKNOWLEDGMENTS

This work was supported by the National Science Foundation under grants CHE-1465049 and CHE-1855240.

DOI: 10.1021/acs.joc.9b01578
J. Org. Chem. 2019, 84, 11649−11664

REFERENCES

(1) Lindsey, J. S. *De Novo* Synthesis of Gem-Dialkyl Chlorophyll Analogues for Probing and Emulating Our Green World. *Chem. Rev.* **2015**, *115*, 6534−6620.

(2) Taniguchi, M.; Lindsey, J. S. Synthetic Chlorins, Possible Surrogates for Chlorophylls, Prepared by Derivatization of Porphyrins. *Chem. Rev.* **2017**, *117*, 344−535.

(3) Scheer, H. In *Chlorophylls*; Scheer, H., Ed.; CRC Press: Boca Raton, FL, 1991; pp 3−30.

(4) (a) Timkovich, R.; Cork, M. S.; Gennis, R. B.; Johnson, P. Y. Proposed structure of heme d, a prosthetic group of bacterial terminal oxidases. *J. Am. Chem. Soc.* **1985**, *107*, 6069−6075. (b) Murshudov, G. N.; Grebenko, A. I.; Barynin, V.; Dauter, Z.; Wilson, K. S.; Vainshtein, B. K.; Melik-Adamyan, W.; Bravo, J.; Ferrán, J. M.; Ferrer, J. C.; et al. Structure of the Heme d of *Penicillium vitale* and *Escherichia coli* Catalases. *J. Biol. Chem.* **1996**, *271*, 8863−8868.

(5) (a) Wang, W.; Kishi, Y. Synthesis and Structure of Tolyporphin A *O,O*-Diacetate. *Org. Lett.* **1999**, *1*, 1129−1132. (b) Brückner, C. Tolyporphin − An Unusual Green Chlorin-like Dioxobacteriochlorin. *Photochem. Photobiol.* **2017**, *93*, 1320−1325.

(6) (a) Weeg-Aerssens, E.; Wu, W.; Ye, R. W.; Tiedje, J. M.; Chang, C. K. Purification of Cytochrome cd1 Nitrite Reductase from Pseudomonas stutzeri JM300 and Reconstitution with Native and Synthetic Heme d_1. *J. Biol. Chem.* **1991**, *266*, 7496−7502. (b) Chang, C. K.; Wu, W. The Porphinedione Structure of Heme d_1. Synthesis and Spectral Properties of Model Compounds of the Prosthetic Group of Dissimilatory Nitrite Reductase. *J. Biol. Chem.* **1986**, *261*, 8593−8596.

(7) Murphy, M. J.; Siegel, L. M.; Tove, S. R.; Kamin, H. Siroheme: A New Prosthetic Group Participating in Six-Electron Reduction Reactions Catalyzed by Both Sulfite and Nitrite Reductases. *Proc. Natl. Acad. Sci.* **1974**, *71*, 612−616.

(8) Ballantine, J. A.; Psaila, A. F.; Pelter, A.; Murray-Rust, P.; Ferrito, V.; Schembri, P.; Jaccarini, V. The Structure of Bonellin and Its Derivatives. Unique Physiologically Active Chlorins from the Marine Echurian *Bonellia Viridis*. *J. Chem. Soc., Perkin Trans. 1* **1980**, 1080−1089.

(9) (a) Pelter, A.; Ballantine, J. A.; Ferrito, V.; Jaccarini, V.; Psaila, A. F.; Schembri, P. J. Bonellin, a Most Unusual Chlorin. *J. Chem. Soc., Chem. Commun.* **1976**, 999−1000. (b) Battersby, A. R.; Dutton, C. J.; Fookes, C. J. R.; Turner, S. P. D. Synthesis of the Chlorin Macrocycle by a Photochemical Approach. *J. Chem. Soc., Chem. Commun.* **1983**, 1237−1238. (c) Montforts, F.-P.; Schwartz, U. M. Total Synthesis of (±)-Bonellin Dimethyl Ester. *Angew. Chem., Int. Ed. Engl.* **1985**, *24*, 775−776.

(10) (a) Karuso, P.; Bergquist, P. R.; Buckleton, J. S.; Cambie, R. C.; Clark, G. R.; Rickard, C. E. F. 13^2,17^3-Cyclopheophorbide Enol, the First Porphyrin Isolated from a Sponge. *Tetrahedron Lett.* **1986**, *27*, 2177−2178. ((b)) Schopf, J. W.. In *Earth's Earliest Biosphere: Its Origin and Evolution*; Schopf, J. W., Ed.; Princeton University Press: Princeton, 1983; p 543. (c) Bible, K. C.; Buytendorp, M.; Zierath, P. D.; Rinehart, K. L. Tunichlorin: a Nickel Chlorin Isolated from the Caribbean Tunicate *Tridemnum Solidum*. *Proc. Natl. Acad. Sci.* **1988**, *85*, 4582−4586. (d) Sakata, K.; Yamamoto, K. I.; Ishikawa, H.; Yagi, A.; Etoh, H.; Ina, K. Chlorophyllone-a, a New Pheophorbide-*a* related Compound Isolated from as an Antioxidative Compound. *Tetrahedron Lett.* **1990**, *31*, 1165−1168. (e) Yamamoto, K. I.; Sakata, K.; Watanabe, N.; Yagi, A.; Brinen, L. S.; Clardy, J. Chlorophyllonic Acid and Methyl Ester, a New Chlorophyll *a* Related Compound Isolated as an Antioxidant from Short-Necked Clam, *Ruditapes Philippinarum*. *Tetrahedron Lett.* **1992**, *33*, 2587−2588. (f) Watanabe, N.; Yamamoto, K. I.; Ishikawa, H.; Yagi, A.; Sakata, K.; Brinen, L. S.; Clardy, J. New Chlorophyll-*a* Related Compounds Isolated as Antioxidants from Marine Bivalves. *J. Nat. Prod.* **1993**, *56*, 305−317. (g) Ma, L.; Dolphin, D. Stereoselective Synthesis of New Chlorophyll *a* Related Antioxidants Isolated from Marine Organisms. *J. Org. Chem.* **1996**, *61*, 2501−2510.

(11) (a) Scott, L. J.; Goa, K. L. Verteporfin. *Drugs Aging* **2000**, *16*, 139−146. (b) Karim, S. P.; Adelman, R. A. Profile of verteporfin and Its Potential for the Treatment of Central serous Chorioretinopathy. *Clin. Ophthalmol.* **2013**, *7*, 1867−1875. (c) Ethirajan, M.; Chen, Y.; Joshi, P.; Pandey, R. K. The Role of Porphyrin Chemistry in Tumor Imaging and Photodynamic Therapy. *Chem. Soc. Rev.* **2011**, *40*, 340−362.

(12) Jain, M.; Zellweger, M.; Frobert, A.; Valentin, J.; Bergh, H. V. D.; Wagnières, G.; Cook, S.; Giraud, M.-N. Intra-Arterial Drug and Light Delivery for Photodynamic Therapy Using Visudyne®: Implication for Atherosclerotic Plaque Treatment. *Front. Physiol.* **2016**, *7*, 400.

(13) (a) Senge, M. O.; Brandt, J. C. Temoporfin (Foscan®, 5,10,15,20-tetra(*m*-hydroxyphenyl)chlorin) - a second-generation photosensitizer. *Photochem. Photobiol.* **2011**, *87*, 1240−1296. (b) Senge, M. O. *Photodiagn. Photodyn. Ther.* **2012**, *9*, 170. (c) de Visscher, S. A. H. J.; Dijkstra, P. U.; Tan, I. B.; Roodenburg, J. L. N.; Witjes, M. J. H. mTHPC Mediated Photodynamic Therapy (PDT) of Squamous Cell Carcinoma in the Head and Neck: a Systematic Review. *Oral Oncol.* **2013**, *49*, 192.

(14) (a) Wang, S.; Bromley, E.; Xu, L.; Chen, J. C.; Keltner, L. Talaporfin Sodium. *Expert Opin. Pharmacother.* **2010**, *11*, 133−140. (b) Miki, Y.; Akimoto, J.; Hiranuma, M.; Fujiwara, Y. Effect of talaporfin sodium-mediated photodynamic therapy on cell death modalities in human glioblastoma T98G cells. *J. Toxicol. Sci.* **2014**, *39*, 821−827.

(15) Liu, Y.; Zhang, S.; Lindsey, J. S. Total Synthesis Campaigns Towards Chlorophylls and Related Natural Hydroporphyrins − Diverse Macrocycles, Unrealized Opportunities. *Nat. Prod. Rep.* **2018**, *35*, 879−901.

(16) (a) Callot, H. J.; Schaeffer, E. Homologation Directe du Cycle des Porphyrines par les Diazoalcanes. *Tetrahedron* **1978**, *34*, 2295−2300. (b) Vogel, E.; Köcher, M.; Balci, M.; Teichler, I.; Lex, J.; Schmickler, H.; Ermer, O. 2,3-Dihydroporphycene − an Analogue of Chlorin. *Angew. Chem., Int. Ed. Engl.* **1987**, *26*, 931−934. (c) McCarthy, J. R.; Jenkins, H. A.; Brückner, C. Free Base *meso*-Tetraarylmorpholinochlorins and Porpholactone from *meso*-Tetraaryl-2,3-dihydroxy-chlorin. *Org. Lett.* **2003**, *5*, 19−22. (d) Lara, K. K.; Rinaldo, C. R.; Brückner, C. *meso*-Tetraaryl-7,8-dihydroxydithiachlorins: First Examples of Heterochlorins. *Tetrahedron Lett.* **2003**, *44*, 7793−7797. (e) Akhigbe, J.; Haskoor, J.; Krause, J. A.; Zeller, M.; Brückner, C. Formation, Structure, and Reactivity of *meso*-Tetraarylchlorolactones, −porpholactams, and −chlorolactams, Porphyrin and Chlorin Analogues Incorporating Oxazolone or Imidazolone Moieties. *Org. Biomol. Chem.* **2013**, *11*, 3616−3628. (f) Ogikubo, J.; Meehan, E.; Engle, J. T.; Ziegler, C. J.; Brückner, C. *meso*-Aryl-3-alkyl-2-oxachlorins. *J. Org. Chem.* **2012**, *77*, 6199−6207.

(17) Lash, T. D. Carbaporphyrinoid Systems. *Chem. Rev.* **2017**, *117*, 2313−2446.

(18) Lash, T. D. Metal Complexes of Carbaporphyrinoid Systems. *Chem. − Asian J.* **2014**, *9*, 682−705.

(19) Hayes, M. J.; Lash, T. D. Carbachlorins. *Chem. − Eur. J.* **1998**, *4*, 508−511.

(20) Li, D.; Lash, T. D. Synthesis and Reactivity of Carbachlorins and Carbaporphyrins. *J. Org. Chem.* **2014**, *79*, 7112−7121.

(21) Sahota, N.; Ferrence, G. M.; Lash, T. D. Synthesis and Properties of Carbaporphyrin and Carbachlorin Dimethyl Esters Derived from Cyclopentanedialdehydes. *J. Org. Chem.* **2017**, *82*, 9715−9730.

(22) Li, D.; Lash, T. D. Synthesis and Oxidation of Internally Chlorinated Carbachlorins. *Eur. J. Org. Chem.* **2017**, 6775−6780.

(23) Lash, T. D. Out of the Blue! Azuliporphyrins and Related Carbaporphyrinoid Systems. *Acc. Chem. Res.* **2016**, *49*, 471−482.

(24) Lash, T. D.; Colby, D. A.; Graham, S. R.; Ferrence, G. M.; Szczepura, L. F. Organometallic Chemistry of Azuliporphyrins: Synthesis, Spectroscopy, Electrochemistry and Structural Characterization of Nickel(II), Palladium(II) and Platinum(II) Complexes of Azuliporphyrins. *Inorg. Chem.* **2003**, *42*, 7326−7338.

(25) Białek, M.; Latos-Grażyński, L. Merging of Inner and Outer Ruthenium Organometallic Coordination Motifs Within an Azuliporphyrin Framework. *Chem. Commun.* **2014**, *50*, 9270−9272.

DOI: 10.1021/acs.joc.9b01578
J. Org. Chem. 2019, 84, 11649−11664

(26) Stateman, L. M.; Ferrence, G. M.; Lash, T. D. Rhodium(III) Azuliporphyrins. *Organometallics* **2015**, *34*, 3842−3848.
(27) Lash, T. D.; Pokharel, K.; Zeller, M.; Ferrence, G. M. Iridium(III) Azuliporphyrins. *Chem. Commun.* **2012**, *48*, 11793−11795.
(28) Lash, T. D.; Chaney, S. T. Azuliporphyrin, a Case of Borderline Porphyrinoid Aromaticity. *Angew. Chem., Int. Ed. Engl.* **1997**, *36*, 839−840.
(29) Lash, T. D.; Colby, D. A.; Graham, S. R.; Chaney, S. T. Synthesis, Spectroscopy, and Reactivity of *meso*-Unsubstituted Azuliporphyrins and Their Heteroanalogues. Oxidative Ring Contractions to Carba-, Oxacarba-, Thiacarba-, and Selenacarbaporphyrins. *J. Org. Chem.* **2004**, *69*, 8851−8864.
(30) Larsen, S.; McCormick-McPherson, L. J.; Teat, S. J.; Ghosh, A. *ACS Omega* **2019**, *4*, 6737−6745.
(31) Richter, D. T.; Lash, T. D. Synthesis of Sapphyrins, Heterosapphyrins, and Carbasapphyrins by a "4 + 1" Approach. *J. Org. Chem.* **2004**, *69*, 8842−8850.
(32) Sasaki, Y.; Takase, M.; Okujima, T.; Mori, S.; Uno, H. Synthesis and Redox properties of Pyrrole- and Azulene-Fused Azacoronene. *Org. Lett.* **2019**, *21*, 1900−1903.
(33) Noboa, M. A.; Lash, T. D. *Abstracts of Papers, 255th ACS National Meeting*. Investigations Directed Towards the Synthesis of Carbachlorins, New Orleans, LA, March 18−22, 2018; American Chemical Society: Washington, DC. 2018; ORGN-633.
(34) Lash, T. D. What's in a Name? The MacDonald Condensation. *J. Porphyrins Phthalocyanines* **2016**, *20*, 855−888.
(35) Jacobi, P. A.; Lanz, S.; Ghosh, I.; Leung, S. H.; Löwer, F.; Pippin, D. A New Synthesis of Chlorins. *Org. Lett.* **2001**, *3*, 831−834.
(36) O'Neal, W. G.; Roberts, W. P.; Ghosh, I.; Jacobi, P. A. Studies in Chlorin Chemistry. II. A Versatile Synthesis of Dihydrodipyrrins. *J. Org. Chem.* **2005**, *70*, 7243−7251.
(37) O'Neal, W. G.; Roberts, W. P.; Ghosh, I.; Wang, H.; Jacobi, P. A. Studies in Chlorin Chemistry. 3. A Practical Synthesis of C,D-Ring Symmetric Chlorins of Potential Utility in Photodynamic Therapy. *J. Org. Chem.* **2006**, *71*, 3472−3480.
(38) O'Nea, W. G.; Jacobi, P. A. Toward a General Synthesis of Chlorins. *J. Am. Chem. Soc.* **2008**, *130*, 1102−1108.
(39) Liu, Y.; Allu, S.; Reddy, M. N.; Hood, D.; Diers, J. R.; Bocian, D. F.; Holten, D.; Lindsey, J. S. Synthesis and Photophysical Characterization of Bacteriochlorins Equipped with Integral Swallowtail Substituents. *New J. Chem.* **2017**, *41*, 4360−4376.
(40) Lash, T. D.; Lammer, A. D.; Idate, A. S.; Colby, D. A.; White, K. Preparation of Azulene-Derived Fulvenedialdehydes and Their Application to the Synthesis of Stable *adj*-Dicarbaporphyrinoids. *J. Org. Chem.* **2012**, *77*, 2368−2381.
(41) Lash, T. D.; El-Beck, J. A.; Ferrence, G. M. Syntheses and Reactivity of *meso*-Unsubstituted Azuliporphyrins Derived from 6-*tert*-Butyl- and 6-Phenylazulene. *J. Org. Chem.* **2007**, *72*, 8402−8415.
(42) Lash, T. D. The Azuliporphyrin-Carbaporphyrin Connection. *Chem. Commun.* **1998**, 1683−1684.
(43) Colby, D. A.; Lash, T. D. Adaptation of the Rothemund Reaction for Carbaporphyrin Synthesis: Preparation of *meso*-Tetraphenylazuliporphyrin and Related Benzocarbaporphyrins. *Chem. − Eur. J.* **2002**, *8*, 5397−5402.
(44) Lash, T. D.; Hayes, M. J.; Spence, J. D.; Muckey, M. A.; Ferrence, G. M.; Szczepura, L. F. Conjugated Macrocycles Related to the Porphyrins. 21. Synthesis, Spectroscopy, Electrochemistry, and Structural Characterization of Carbaporphyrins. *J. Org. Chem.* **2002**, *67*, 4860−4874.
(45) Grabowski, E. Y.; AbuSalim, D. I.; Lash, T. D. Naphtho[2,3-b]carbaporphyrins. *J. Org. Chem.* **2018**, *83*, 11825−11838.
(46) (a) Ghosh, A. First-principles Quantum Chemical Studies of Porphyrins. *Acc. Chem. Res.* **1998**, *31*, 189−198. ((b)) Ghosh, A. Quantum Chemical Studies of Molecular Structures and Potential Energy Surfaces of Porphyrins and Hemes.*The Porphyrin Handbook*; Kadish, K. M.; Smith, K. M.; Guilard, R., Eds.; Academic Press: San Diego, 2000; Vol. 7, pp 1−38.
(47) Alonso, M.; Geerlings, P.; De Proft, F. Exploring the Structure-Aromaticity Relationship in Hückel and Möbius N-Fused Pentaphyrins using DFT. *Phys. Chem. Chem. Phys.* **2014**, *16*, 14396−14407.
(48) Alonso, M.; Geerlings, P.; De Proft, F. Topology Switching in [32]Heptaphyrins Controlled by Solvent, Protonation, andmeso Substituents. *Chem. − Eur. J.* **2013**, *19*, 1617−1628.
(49) Schleyer, P. v. R.; Maerker, C.; Dransfeld, A.; Jiao, H.; van Eikema Hommes, N. J. R. Nucleus-Independent Chemical Shifts: a Simple and Efficient Aromaticity Probe. *J. Am. Chem. Soc.* **1996**, *118*, 6317−6318.
(50) Geuenich, D.; Hess, K.; Köhler, F.; Herges, R. Anisotropy of the Induced Current Density (ACID), a General Method to Quantify and Visualize Electronic Delocalization. *Chem. Rev.* **2005**, *105*, 3758−3772.
(51) AbuSalim, D. I.; Lash, T. D. Tropylium and Porphyrinoid Character in Carbaporphyrinoid Systems. Relative Stability and Aromatic Characteristics of Azuliporphyrin and Tropiporphyrin Tautomers, Protonated Species, and Related Structures. *J. Phys. Chem. A* **2019**, *123*, 230−246.
(52) Jayasundera, K. P.; Kinoshita, H.; Inomata, K. An Efficient Method to Construct the A,B-Rings Component toward Total Syntheses of and Its Derivative as a Photoprobe. *Bull. Chem. Soc. Jpn.* **2000**, *73*, 497−505.
(53) Clezy, P. S.; Crowley, R. J.; Hai, T. T. The Chemistry of Pyrrolic Compounds. L. The Synthesis of Oxorhodoporphyrin Dimethyl Ester and Some of Its Derivatives. *Aust. J. Chem.* **1982**, *35*, 411−421.
(54) Frisch, M. J.; Trucks, G. W.; Schlegel, H. B.; Scuseria, G. E.; Robb, M. A.; Cheeseman, J. R.; Scalmani, G.; Barone, V.; Petersson, G. A.; Nakatsuji, H.; et al.. *Gaussian 09, Revision D.01*; Gaussian, Inc., Wallingford, CT, 2016.
(55) Becke, A. D. Density Functional Thermochemistry. III. The Exact Role of Exchange. *J. Chem. Phys.* **1993**, *98*, 5648−5652.
(56) Lee, C.; Yang, W.; Parr, R. G. Development of the Colle-Salvetti Correlation-Energy Formula into a Functional of the Electron Density. *Phys. Rev. B: Condens. Matter Mater. Phys.* **1988**, *37*, 785−789.
(57) Vosko, S. H.; Wilk, L.; Nusair, M. Accurate Spin-Dependent Electron Liquid Correlation Energies for Local Spin Density Calculations: A Critical Analysis. *Can. J. Phys.* **1980**, *58*, 1200−1211.
(58) Stephens, P. J.; Devlin, F. J.; Chabalowski, C. F.; Frisch, M. J. *Ab Initio* Calculation of Vibrational Absorption and Circular Dichroism Spectra using Density Functional Force Fields. *J. Phys. Chem.* **1994**, *98*, 11623−11627.
(59) Grimme, S.; Antony, J.; Ehrlich, S.; Krieg, H. A Consistent and Accurate Ab Initio Parametrization of Density Functional Dispersion Correction (DFT-D) for the 94 Elements H-Pu. *J. Chem. Phys.* **2010**, *132*, 154104.
(60) Zhao, Y.; Truhlar, D. G. The M06 Suite of Density Functionals for Main Group Thermochemistry, Thermochemical Kinetics, Noncovalent Interactions, Excited States, and Transition Elements: Two New Functionals and Systematic Testing of Four M06-Class Functionals and 12 Other Functionals. *Theor. Chem. Acc.* **2008**, *120*, 215−241.
(61) Wolinski, K.; Hinton, J. F.; Pulay, P. Efficient Implementation of the Gauge-independent Atomic Orbital Method for NMR Chemical Shift Calculations. *J. Am. Chem. Soc.* **1990**, *112*, 8251−8260.
(62) Herges, R.; Geuenich, D. Delocalization of Electrons in Molecules. *J. Phys. Chem. A* **2001**, *105*, 3214−3220.

DOI: 10.1021/acs.joc.9b01578
J. Org. Chem. 2019, 84, 11649−11664